



On the use of finite fault solution for tsunami generation problems

Denys Dutykh, Dimitrios Mitsotakis, Xavier Gardeil, Frédéric Dias

► To cite this version:

Denys Dutykh, Dimitrios Mitsotakis, Xavier Gardeil, Frédéric Dias. On the use of finite fault solution for tsunami generation problems. Theoretical and Computational Fluid Dynamics, 2013, 27 (1), pp.177-199. 10.1007/s00162-011-0252-8 . hal-00509384v3

HAL Id: hal-00509384

<https://hal.science/hal-00509384v3>

Submitted on 12 Dec 2011

HAL is a multi-disciplinary open access archive for the deposit and dissemination of scientific research documents, whether they are published or not. The documents may come from teaching and research institutions in France or abroad, or from public or private research centers.

L'archive ouverte pluridisciplinaire **HAL**, est destinée au dépôt et à la diffusion de documents scientifiques de niveau recherche, publiés ou non, émanant des établissements d'enseignement et de recherche français ou étrangers, des laboratoires publics ou privés.



Distributed under a Creative Commons Attribution - NonCommercial - ShareAlike| 4.0 International License

ON THE USE OF THE FINITE FAULT SOLUTION FOR TSUNAMI GENERATION PROBLEMS

DENYS DUTYKH*, DIMITRIOS MITSOTAKIS, XAVIER GARDEIL, AND FRÉDÉRIC DIAS

ABSTRACT. The present study is devoted to the problem of tsunami wave generation. The main goal of this work is two-fold. First of all, we propose a simple and computationally inexpensive model for the description of the sea bed displacement during an underwater earthquake, based on the finite fault solution for the slip distribution under some assumptions on the dynamics of the rupturing process. Once the bottom motion is reconstructed, we study waves induced on the free surface of the ocean. For this purpose we consider three different models approximating the Euler equations of the water wave theory. Namely, we use the linearized Euler equations (we are in fact solving the Cauchy-Poisson problem), a Boussinesq system and a novel weakly nonlinear model. An intercomparison of these approaches is performed. The developments of the present study are illustrated on the 17 July 2006 Java event, where an underwater earthquake of magnitude 7.7 generated a tsunami that inundated the southern coast of Java.

1. INTRODUCTION

Tsunami waves have attracted a lot of attention by researchers. The interest of the scientific community has especially increased after the two megatsunamis in December 2004 [SB06], where nearly 230,000 people in fourteen countries lost their lives, and in March 2011, where 20,000 people lost their lives in Japan. The 2004 event also led Indian Ocean countries to develop Tsunami Warning Systems (TWS) [Syn05, Bas06], unfortunately more on an individual basis than on a collective basis. The most elaborated warning system to date is the Pacific Ocean TWS, which has been developed over several decades by efforts of NOAA's specialists [TGB⁺05, GBM⁺05].

An operational tsunami wave modeling tool is an essential part of any warning system [TGB⁺05, TDS07]. Mathematical and numerical models in use should be constantly improved to produce more accurate results in less CPU time [Ima96, TG97, DPD11]. In order to study the propagation of a tsunami wave, an initial condition must usually be provided to any numerical model designed for this purpose. The present study is an attempt to improve the construction of the initial tsunami waveform. The set of existing practices described in the literature constitutes the field of the so-called tsunami generation modeling [Ham73, TT01, DD07d, Dut07, DD09, DD10].

The modeling of tsunami generation was initiated in the early sixties by the prominent work of Kajiura [Kaj63], who proposed the translation of the static sea bed displacement

Key words and phrases. water waves; tsunami waves; co-seismic displacements; moving bottom; tsunami generation.

* Corresponding author.

towards the free surface as an initial condition. Classically, the celebrated Okada [Oka85, Oka92] and sometimes Mansinha & Smylie¹ [MS67, MS71] solutions are used to compute the co-seismic sea bed displacements. This approach is still widely used by the tsunami wave modeling community. However, significant progress has been recently made in this direction [OTM01, DD07d, Dut07, DD09, RLF⁺08, SF09, DPD11].

In the present study we exploit some recent advances in seismology to reconstruct better co-seismic displacements of a tsunamigenic earthquake. More precisely, we suggest using the so-called finite fault solution developed by Ji and his collaborators [BLM00, JWH02], based on static and seismic data inversion. This solution provides multiple fault segments of variable local slip, rake angle and several other parameters. By applying Okada's solution to each subfault, we reconstruct the sea bed displacement with higher resolution. To our knowledge, this technique has already been employed to model the Kuril islands tsunamis of 15 November 2006 and 13 January 2007, cf. [RLF⁺08]. Since Okada's solution consists of relatively simple closed-form analytical expressions, all computations can be done efficiently enough so that they can be used in a real-time TWS (cf. [WL08]). The obvious *sine qua non* condition is that the corresponding finite fault inversion should also be performed in a reasonable time.

In the present study we go further in reconstructing the dynamic sea bed displacement according to the rupture propagation speed and the rise time also provided by the finite fault solution. Constructed in this special way, sea bed displacements are then coupled with several water wave models. Among them, there is a novel weakly nonlinear solver based on a formulation involving the Dirichlet-to-Neumann operator which is computed approximately using Fourier transforms. The other two models considered here are the linearized free surface Euler equations and a Boussinesq type system. Developments presented in this paper are illustrated on the example of July 17, 2006 Java event [AKLV06]. However, we would like to stress that the methodology presented in this study is quite general and can be applied to many other tsunamigenic earthquakes for which a finite fault solution is available.

The paper is organized as follows. In Section 2 we describe the static and dynamic sea bed displacements, while in Section 3 we present a simple approximate water wave solver with a moving bottom. In Section 4 we study numerically the generation process of a real-world event. An intercomparison of the three models mentioned above is performed. Some important conclusions are drawn in Section 5.

2. CO-SEISMIC DISPLACEMENT CONSTRUCTION

The modeling of tsunami generation is directly related to the problem of the bottom motion during an underwater earthquake. Traditionally, Okada's solution [Oka85, Oka92] is used in regimes characterized by an active fault of small or intermediate size, i.e. consisting of one or a few segments (e.g. the great Sumatra 2004 earthquake, [SB06, IAK⁺07]). In this case the resulting vertical displacement field is translated to the free surface. This approach is conventionally referred to as *passive tsunami generation* [DDK06], contrary to

¹In fact, the Mansinha & Smylie solution is a particular case of the more general Okada solution.

Fault length, km	80.9
Fault width, km	40.0
Focal depth, km	20.0
Slip, m	2.5
Dip angle	10°
Slip angle	95°
Strike angle (clockwise from N)	289°

TABLE 1. Seismic fault parameters for the Java 2006 event. The corresponding seismic moment can be taken as $M_0 = 2.52 \times 10^{27}$ N·m ($M_w = 7.56$).

the *active generation* which explicitly involves the bottom motion dynamics [DD07d]. Since our methods will be illustrated on the example of the July 17, 2006 Java event, we show in Figure 1 a typical single-fault based initial condition used for the corresponding tsunami wave modeling [Yal08]. The seismic parameters used to produce this vertical displacement are given in Table 1.

Remark 1. *The celebrated Okada solution [Oka85, Oka92] is based on two main ingredients — the dislocation theory of Volterra [Vol07] and Mindlin’s fundamental solution for an elastic half-space [Min36]. Particular cases of this solution were known before Okada’s work, for example the well-known Mansinha & Smylie’s solution [MS67, MS71]. Usually, all these particular cases differ by the choice of the dislocation and Burger’s vector orientation [Pre65]. We recall the basic assumptions behind this solution:*

- *The fault is immersed into a linear homogeneous and isotropic half-space*
- *The fault is a Volterra type dislocation*
- *The dislocation has a rectangular shape*

For more information on Okada’s solution we refer to [DD07d, DD07a, Dut07].

The finite fault solution is based on the multi-fault representation of the rupture [BLM00, JWH02]. The rupture complexity is reconstructed using a joint inversion of the static and seismic data. The fault’s surface is parametrized by multiple segments with variable local slip, rake angle, rise time and rupture velocity. The inversion is performed in an appropriate wavelet transform space. The objective function is a weighted sum of L_1 , L_2 norms and some correlative functions. With this approach seismologists are able to recover rupture slip details [BLM00, JWH02]. This available seismic information is exploited in this study to compute the sea bed displacements produced by an underwater earthquake with higher geophysical resolution.

The proposed approach will be directly illustrated on the Java 2006 event. The July 17, 2006 Java earthquake involved thrust faulting in the Java trench and generated a tsunami wave that inundated the southern coast of Java [AKLV06, FKM⁺07]. The estimates of the size of the earthquake (cf. [AKLV06]) indicate a seismic moment of 6.7×10^{20} N·m, which corresponds to the magnitude $M_w = 7.8$. Later this estimate was refined to $M_w = 7.7$ [Ji06]. Like other events in this region, this 2006 event had an unusually low

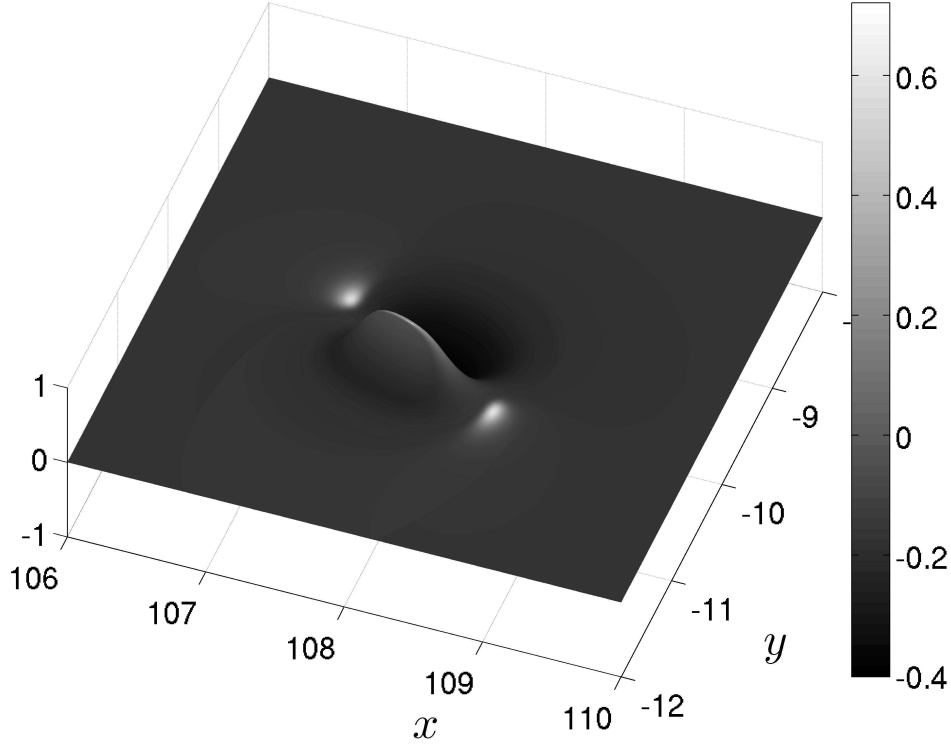


FIGURE 1. Static vertical displacement in meters of the seabed computed with the single fault parameters provided in Table 1. The maximum lift is 0.7215 m while the maximum subsidence is 0.4030 m. The x -axis is the longitude while the y -axis is the latitude. The y -axis points to the North.

rupture speed of 1.0 – 1.5 km/s, and occurred near the up-dip edge of the subduction zone thrust fault. According to Ammon *et al*, most aftershocks involved normal faulting [AKLV06]. The rupture propagated approximately 200 km along the trench with an overall duration of approximately 185 s. The fault's surface projection along with ocean ETOPO1 bathymetric map are shown in Figure 2. We note that the Indian Ocean bathymetry considered in this study varies between 7186 and 20 meters in the shallowest region.

Remark 2. *The estimate of the finite fault inversion for this earthquake was also performed by the Caltech team [Ozg06]. The magnitude estimated in that study was $M_w = 7.9$. In this study we do not present numerical simulations using their data but it is straightforward to apply our algorithms to this case as well.*

2.1. Static displacement. In order to illustrate the advantages of the proposed approach we will also compute the static co-seismic displacements using the finite fault solution [Ji06]. The fault is considered to be the rectangle with vertices located at (109.20508° (Lon), -10.37387° (Lat), 6.24795 km (Depth)), (106.50434°, -9.45925°, 6.24795 km), (106.72382°,

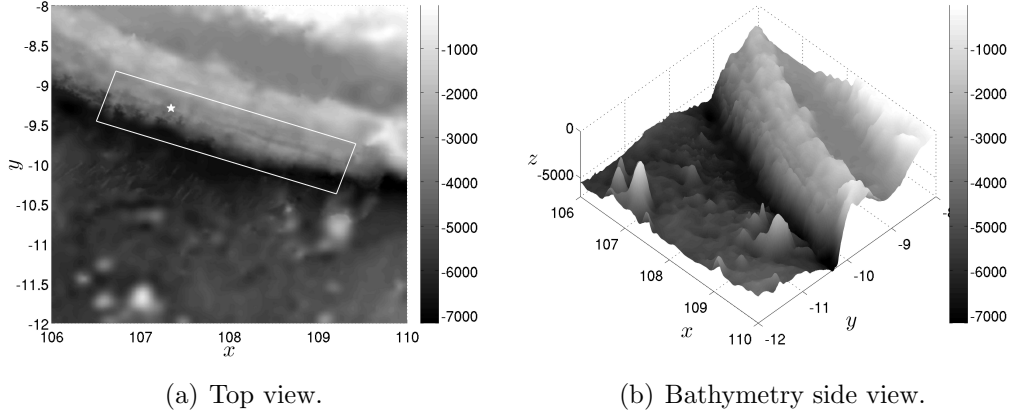


FIGURE 2. Surface projection of the fault’s plane and the ETOPO1 bathymetric map of the region under investigation. The symbol \star indicates the epicenter’s location at $(107.345^\circ, -9.295^\circ)$. The local Cartesian coordinate system is centered at the point $(108^\circ, -10^\circ)$. The region is located between $(106^\circ, -8^\circ)$ and $(110^\circ, -12^\circ)$.

P -wave celerity c_p , m/s	6000
S -wave celerity c_s , m/s	3400
Crust density ρ , kg/m ³	2700
Dip angle, δ	10.35°
Strike angle (clockwise from N)	289°

TABLE 2. Geophysical parameters used to model elastic properties of the subduction zone in the region of Java.

-8.82807° , 19.79951 km), $(109.42455^\circ, -9.74269^\circ, 19.79951$ km) (see Figure 2a). The fault’s plane is conventionally divided into $N_x = 21$ subfaults along strike and $N_y = 7$ subfaults down the dip angle, leading to a total number of $N_x \times N_y = 147$ equal segments. Parameters such as subfault location (x_c, y_c) , depth d_i , slip u and rake angle ϕ for each segment are given in Table 3 and can also be downloaded from [Ji06]. The elastic constants common to all subfaults and parameters such as dip and slip angles are given in Table 2. (We note that the slip angle is measured conventionally in the counter-clockwise direction from the North. The relations between the elastic wave celerities c_p , c_s and the Lamé coefficients λ , μ used in Okada’s solution are given in Appendix C.)

We compute Okada’s solution at the sea bottom by substituting $z = 0$ in the geophysical coordinate system and taking the vertical component of the displacement field $\mathcal{O}_i(\vec{x}; \delta, \lambda, \mu, \dots)$, where δ is the dip angle, λ , μ are the Lamé coefficients (see Appendix C) and the dots denote the dependence of the function $\mathcal{O}(\vec{x})$ on eight other parameters, cf. [DD07d]. The resulting co-seismic vertical bottom displacement $\zeta(\vec{x})$ can be computed as

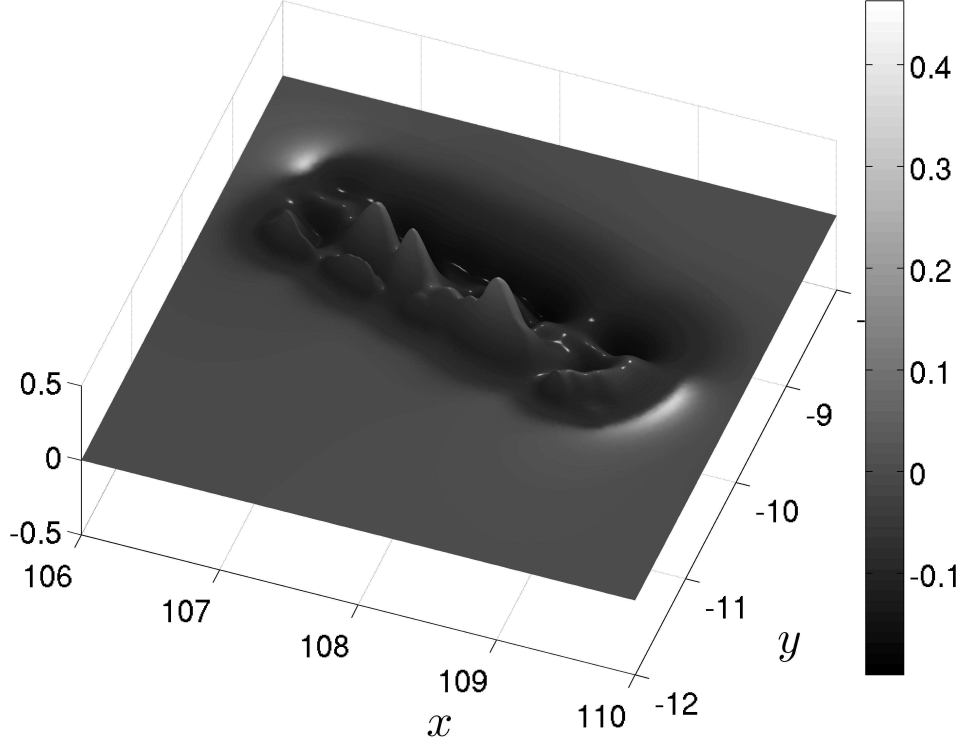


FIGURE 3. The vertical displacement of the finite fault solution, cf. [Ji06]. The corresponding seismic moment is $M_0 = 3.53 \times 10^{27}$ N·m ($M_w = 7.65$). The maximum lift is 0.4629 while the maximum subsidence is 0.1997.

a simple superposition of subfault contributions:

$$\zeta(\vec{x}) = \sum_{i=1}^{N_x \times N_y} \mathcal{O}_i(\vec{x}; \delta, \lambda, \mu, \dots)$$

The graph of $\zeta(\vec{x})$ is presented in Figure 3. The specific static displacement can be compared with the single fault classical approach depicted on Figure 1. It is worth mentioning that more than one local extrema can be found in this solution due to a higher slip resolution.

Hereafter we will adopt the short-hand notation $\mathcal{O}_i(\vec{x})$ for the vertical displacement component of Okada's solution for the i^{th} segment having in mind its dependence on various parameters from Tables 2 and 3.

2.2. Dynamic co-seismic displacements. Here, we go even further in the reconstruction of the bottom motion. By making some assumptions on the time dependence of the displacement fields, we can have an insight into the dynamics of the sea bed motion.

The finite fault solution provides two additional parameters concerning the rupture dynamics for the July 17, 2006 event — the rupture velocity $v_r = 1.1$ km/s and the rise time $t_r = 8$ s. The epicenter is located at the point $\vec{x}_e = (107.345^\circ, -9.295^\circ)$ [Ji06]. Given the origin \vec{x}_e , the rupture velocity v_r and the i^{th} subfault location \vec{x}_i (the full list is provided in Table 3), we define the *subfault activation times* t_i needed for the rupture to reach the corresponding segment i by the formula:

$$t_i = \frac{\|\vec{x}_e - \vec{x}_i\|}{v_r}, \quad i = 1, \dots, N_x \times N_y.$$

For the sake of simplicity and due to the lack of information we assume implicitly that the rupture speed v_r is constant along the fault; however this can be refined in future studies.

We will also follow the pioneering idea of J. Hammack [Ham72, Ham73] developed later in [TT01, THT02, DD07d, DDK06, KDD07] where the maximum bottom deformation is achieved during some finite time (known as the rise time) according to a specific (in an *ad hoc* manner) dynamic scenario. Various scenarios on the time dependence (instantaneous, linear, trigonometric, exponential, etc) can be found in [Ham73, DDK06, DD07d]. In this study we will adopt the trigonometric scenario which can be described by the formula:

$$T(t) = \mathcal{H}(t - t_r) + \frac{1}{2}\mathcal{H}(t)\mathcal{H}(t_r - t)(1 - \cos(\pi t/t_r)),$$

where $\mathcal{H}(t)$ is the Heaviside step function. For illustrative purposes this dynamic scenario is represented on Figure 4. Physically the function $T(t)$ represents the time history of the vertical bottom displacement in terms of its final amplitude. We assume that during the rise time temporal interval $[0, t_r]$ the vertical displacement goes from zero to its final stage according to the trigonometric scenario.

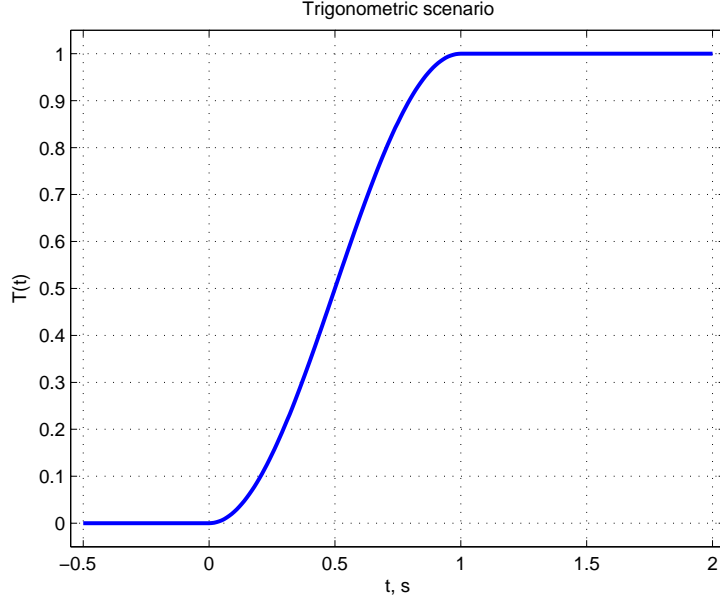
Finally, we put together all the ingredients in order to construct the dynamic sea bed motion:

$$\zeta(\vec{x}, t) = \sum_{i=1}^{N_x \times N_y} \mathcal{H}(t - t_i)T(t - t_i)\mathcal{O}_i(\vec{x}). \quad (2.1)$$

In the following sections we will present several approaches to couple this dynamic deformation with the hydrodynamic problem to predict waves induced on the ocean's free surface.

3. FLUID LAYER SOLUTION

Once the sea bed deformation is determined, a water wave problem must be solved in order to compute the free surface motion induced by the ocean bottom shaking. Traditionally this difficulty is circumvented by the simple translation of the static bottom deformation onto the free surface [Kaj63], known as the passive generation approach [DDK06, KDD07]. In this section we present three approximate models to the water wave problem with moving bottom that we will use in combination with the finite-fault solution to study the tsunami generation problem.

FIGURE 4. Trigonometric scenario with rise time $t_r = 1$ s.

3.1. Linearized Euler equations – CP model. Consider an ideal incompressible fluid of constant density ρ . The horizontal projection of the fluid domain Ω is a subset of \mathbb{R}^2 . The horizontal independent variables are denoted by $\vec{x} = (x, y)$ and the vertical one by z . The origin of the cartesian coordinate system is chosen such that the surface $z = 0$ corresponds to the still water level. The fluid is bounded below by the bottom $z = -h(\vec{x}, t)$ and above by the free surface $z = \eta(\vec{x}, t)$. Usually we assume that the total depth $H(\vec{x}, t) := h(\vec{x}, t) + \eta(\vec{x}, t)$ remains positive $H(\vec{x}, t) \geq h_0 > 0$ at all times $t \in [0, T]$. The sketch of the physical domain is shown in Figure 5.

Remark 3. *Classically in water wave modeling, we make the assumption that the free surface is a graph $z = \eta(\vec{x}, t)$ of a single-valued function. It means in practice that we exclude some interesting phenomena, (e.g. wave breaking phenomena) which are out of the scope of this modeling paradigm.*

The linearized water wave problem consists of the following set of equations [Ham72, Ham73, DD07d]:

$$\Delta\phi = \nabla^2\phi + \partial_{zz}^2\phi = 0, \quad (\vec{x}, z) \in \Omega \times [-h, 0], \quad (3.1)$$

$$\partial_t\eta - \partial_z\phi = 0, \quad z = 0, \quad (3.2)$$

$$\partial_t\phi + g\eta = 0, \quad z = 0, \quad (3.3)$$

$$\partial_th + \partial_z\phi = 0, \quad z = -h(\vec{x}, t). \quad (3.4)$$

This set of equations together with an initial condition is also often referred to in the literature as the Cauchy-Poisson (CP) problem after the pioneering work of Cauchy [Cau27].

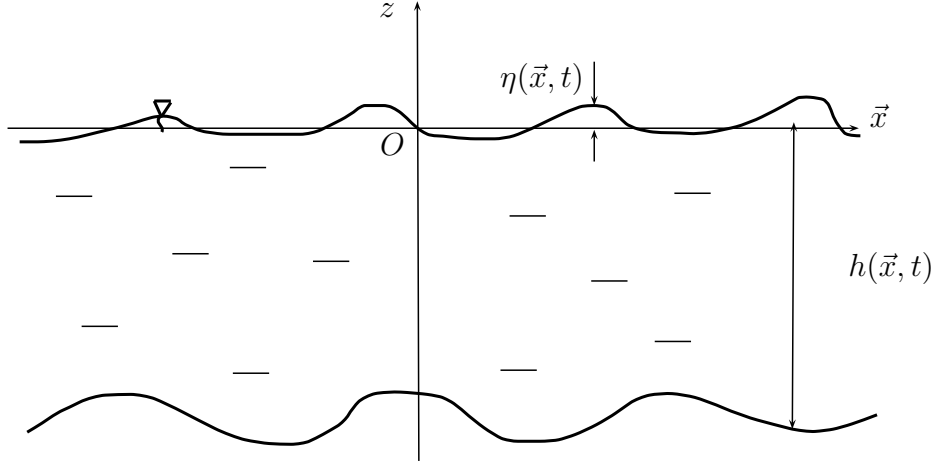


FIGURE 5. Sketch of the physical domain.

In view of the specific requirements of the analytical techniques used in the applications, we will assume first that the domain $\Omega = \mathbb{R}^2$, i.e. it is unbounded in the horizontal extent, and the bottom has a special form:

$$h(\vec{x}, t) = h_0 - \zeta(\vec{x}, t),$$

where h_0 is some uniform depth and $\zeta(\vec{x}, t)$ is the sea bed displacement due to an underwater earthquake. In Section 2.2 one possible construction of the bottom displacement was proposed. Using integral transform methods (cf. [Ham73, TT01, DD07d, KDD07]), one can derive the following expression for the free surface elevation $\eta(\vec{x}, t)$:

$$\eta(\vec{x}, t) = \frac{\gamma^2}{2} \mathcal{F}^{-1} \left\{ \sum_{i=1}^{n=N_x \times N_y} \frac{\mathcal{H}(t - t_i) \hat{\mathcal{O}}_i(\vec{k})}{(\gamma^2 - \omega^2) \cosh(|\vec{k}| h_0)} (\cos(\omega(t - t_i)) - \cos(\gamma(t - t_i))) + \right. \\ \left. \mathcal{H}(t - t_i - t_r) [\cos(\omega(t - t_i - t_r)) + \cos(\gamma(t - t_i))] \right\},$$

where t_r is the rise time defined in Section 2.2, $\gamma = \pi/t_r$,

$$\omega^2 = g|\vec{k}| \tanh(|\vec{k}| h_0)$$

and \mathcal{F}^{-1} is the inverse Fourier transform (see equation (3.13) below). A similar expression can also be derived for the velocity potential $\phi(\vec{x}, z, t)$, however we do not directly need it in our study.

This analytical solution will be used below in numerical simulations. It has the advantage of being simple and, thus, computationally inexpensive. However, the flat bottom assumption ($h(\vec{x}) = h_0 = \text{const}$) prevents us from using this solution beyond some small evolution times. The validity of this approximation has already been addressed in the literature [KDD07, SF09] and will be discussed at some point below.

3.2. The weakly nonlinear (WN) model. A tsunami wave during its generation is usually well described by the Cauchy-Poisson problem [DD07d, KDD07, SF09]. The main reason for this simplification is the fact that a wave of a half meter amplitude represents only a tiny perturbation of over a 4000 m water column. However, the real world bathymetry is generally complex and may contain simultaneously various scales. For example, the subduction zone bathymetry represented on Figure 2 ranges from 7000 to 20 m and thus, nonlinear effects may be locally important. In order to take into account all realistic bathymetric features and study in detail the initial stages of tsunami propagation we describe below a new numerical model.

We consider the physical setting and notation of Section 3.1. The governing equations of the classical water wave problem are the following [Lam32, Sto58, Mei94, Whi99]:

$$\Delta\phi = \nabla^2\phi + \partial_{zz}^2\phi = 0, \quad (\vec{x}, z) \in \Omega \times [-h, \eta], \quad (3.5)$$

$$\partial_t\eta + \nabla\phi \cdot \nabla\eta - \partial_z\phi = 0, \quad z = \eta(\vec{x}, t), \quad (3.6)$$

$$\partial_t\phi + \frac{1}{2}|\nabla\phi|^2 + \frac{1}{2}(\partial_z\phi)^2 + g\eta = 0, \quad z = \eta(\vec{x}, t), \quad (3.7)$$

$$\partial_th + \nabla\phi \cdot \nabla h + \partial_z\phi = 0, \quad z = -h(\vec{x}, t), \quad (3.8)$$

with ϕ the velocity potential, g the acceleration due to gravity force and $\nabla = (\partial_x, \partial_y)$ denotes the gradient operator in horizontal Cartesian coordinates.

The assumptions of fluid incompressibility and flow irrotationality lead to the Laplace equation (3.5) for the velocity potential $\phi(\vec{x}, z, t)$. The main difficulty of the water wave problem lies on the boundary conditions. Equations (3.6) and (3.8) express the free-surface kinematic condition and bottom impermeability respectively, while the dynamic condition (3.7) expresses the free surface isobaricity.

The bathymetry $h(\vec{x}, t)$ is decomposed into the static part $h_0(\vec{x})$ (given e.g. by the ETOPO1 database, cf. Figure 2) and the dynamic sea bed displacement $\zeta(\vec{x}, t)$ constructed above in (2.1):

$$h(\vec{x}, t) = h_0(\vec{x}) - \zeta(\vec{x}, t). \quad (3.9)$$

Remark 4. *Recently, some weak dissipative effects have also been included into the classical water wave problem (3.5) – (3.8). For more details on the visco-potential formulation we refer to [DDZ08, DD07c, Dut07, Dut09b, Dut09a].*

In the sequel we will need the unit exterior normals to the fluid domain. It is straightforward to obtain the following expressions for the normals at the free surface and bottom respectively:

$$\hat{n}_f = \frac{1}{\sqrt{1 + |\nabla\eta|^2}}[-\nabla\eta, 1]^t, \quad \hat{n}_b = \frac{1}{\sqrt{1 + |\nabla h|^2}}[-\nabla h, -1]^t.$$

In 1968 Zakharov proposed a different formulation of the water wave problem based on the trace of the velocity potential at the free surface [Zak68]:

$$\varphi(\vec{x}, t) := \phi(\vec{x}, \eta(\vec{x}, t), t). \quad (3.10)$$

This variable plays the role of generalized momentum in the Hamiltonian description of water waves [Zak68, DB06]. The second canonical variable is the free surface elevation η .

Another important ingredient is the normal velocity at the free surface v_n which is defined as:

$$v_n(\vec{x}, t) := \sqrt{1 + |\nabla\eta|^2} \frac{\partial\phi}{\partial\hat{n}_f} \Big|_{z=\eta} = (\partial_z\phi - \nabla\phi \cdot \nabla\eta)|_{z=\eta}. \quad (3.11)$$

The boundary conditions (3.6) and (3.7) on the free surface can be rewritten in terms of φ , v_n and η [CSS92, CS93, FCKG05]:

$$\begin{aligned} \partial_t\eta - \mathcal{D}_\eta(\varphi) &= 0, \\ \partial_t\varphi + \frac{1}{2}|\nabla\varphi|^2 + g\eta - \frac{1}{2(1+|\nabla\eta|^2)} [\mathcal{D}_\eta(\varphi) + \nabla\varphi \cdot \nabla\eta]^2 &= 0. \end{aligned} \quad (3.12)$$

Here we introduced the Dirichlet-to-Neumann operator (D2N) $\mathcal{D}_\eta : \varphi \mapsto v_n$ [CM85, CS93] which maps the velocity potential at the free surface φ to the normal velocity v_n . The name of this operator comes from the fact that it denotes a correspondance between Dirichlet data φ and Neumann data $\sqrt{1 + |\nabla\eta|^2} \frac{\partial\phi}{\partial\hat{n}_f} \Big|_{z=\eta}$ on the free surface. We provide in Appendix B the complete derivation of Zakharov's formulation for the water wave problem.

3.2.1. Numerical evaluation of the D2N operator. We saw above that the water wave problem can be reduced to a system of two PDEs governing the evolution of the canonical variables η and φ . In order to solve this system of equations we must be able to compute efficiently the quantity $\mathcal{D}_\eta(\varphi)$. In this section we present a simple method for the numerical computation of the D2N operator, which is appropriate for the application of the linearized Euler model in the solution of problems dealing with tsunami generation. This approach is based on the extensive use of Fourier transforms. On the discrete level this transformation can be efficiently implemented with the Fast Fourier Transform (FFT) algorithm [CT65, FJ05].

The direct \mathcal{F} and inverse \mathcal{F}^{-1} Fourier transforms in 2D are defined as follows:

$$\mathcal{F}[f] = \hat{f}(\vec{k}) = \int_{\mathbb{R}^2} f(\vec{x}) e^{-i\vec{k} \cdot \vec{x}} d\vec{x}, \quad \mathcal{F}^{-1}[\hat{f}] = f(\vec{x}) = \frac{1}{(2\pi)^2} \int_{\mathbb{R}^2} \hat{f}(\vec{k}) e^{i\vec{k} \cdot \vec{x}} d\vec{k}. \quad (3.13)$$

The problem to be solved is

$$\nabla^2\phi + \partial_{zz}^2\phi = 0, \quad (\vec{x}, z) \in \Omega \times [-h, \eta], \quad (3.14)$$

$$\phi = \varphi, \quad z = \eta, \quad (3.15)$$

$$\sqrt{1 + |\nabla h|^2} \frac{\partial\phi}{\partial\hat{n}_b} = \partial_t h, \quad z = -h. \quad (3.16)$$

Once the function ϕ is determined, we must compute its normal derivative on the free surface (3.11).

Since a tsunami wave induces a special flow regime in which the horizontal extent is much more important than the variations in the vertical direction, we can apply the Fourier transform to the Laplace equation (3.14) as if it were posed in a strip-like domain:

$$\frac{d^2\hat{\phi}}{dz^2} - |\vec{k}|^2\hat{\phi} = 0.$$

The general exact solution to this ODE can be easily computed:

$$\hat{\phi}(\vec{k}; z) = A(\vec{k}) \cosh(|\vec{k}|z) + B(\vec{k}) \sinh(|\vec{k}|z). \quad (3.17)$$

The two unknown functions $A(\vec{k})$ and $B(\vec{k})$ must be determined from the boundary conditions (3.15), (3.16). For the sake of convenience we rewrite the Neumann boundary condition at the bottom (3.16) in this form:

$$\left. \frac{\partial \phi}{\partial z} \right|_{z=-h} = -\partial_t h - \nabla \phi|_{z=-h} \cdot \nabla h \equiv f(\vec{x}, t). \quad (3.18)$$

The right-hand side will be denoted by $f(\vec{x}, t)$, which implicitly depends on the solution ϕ .

The application of the boundary conditions leads to the following system of linear equations:

$$\begin{aligned} \cosh(|\vec{k}|\eta)A(\vec{k}) + \sinh(|\vec{k}|\eta)B(\vec{k}) &= \hat{\varphi} \\ -|\vec{k}|\sinh(|\vec{k}|h)A(\vec{k}) + |\vec{k}|\cosh(|\vec{k}|h)B(\vec{k}) &= \hat{f}, \end{aligned}$$

which can be easily solved:

$$A(\vec{k}) = \frac{\hat{\varphi} \cosh(|\vec{k}|h) - \hat{f} \frac{\sinh(|\vec{k}|\eta)}{|\vec{k}|}}{\cosh(|\vec{k}|H)}, \quad B(\vec{k}) = \frac{\hat{\varphi} \sinh(|\vec{k}|h) + \hat{f} \frac{\cosh(|\vec{k}|\eta)}{|\vec{k}|}}{\cosh(|\vec{k}|H)}.$$

Here, $H = h + \eta$ is the total water depth. The knowledge of these functions provides the velocity potential in the whole domain thanks to the general solution (3.17).

Finally, we compute the normal velocity v_n on the free surface (3.11). If we compute this quantity in Fourier space, the answer will be given immediately by the inverse transform \mathcal{F}^{-1} . The first term of v_n is readily given by the formula

$$\partial_z \hat{\phi} \Big|_{z=\eta} = \hat{\varphi} |\vec{k}| \tanh(|\vec{k}|H) + \hat{f} \operatorname{sech}(|\vec{k}|H).$$

To compute the second term we use the following approximate expression:

$$\nabla \widehat{\phi|_{z=\eta}} \cdot \nabla \eta = \mathcal{F} \left[\mathcal{F}^{-1} [i\vec{k}\hat{\varphi}] \cdot \mathcal{F}^{-1} [i\vec{k}\hat{\eta}] \right]. \quad (3.19)$$

Remark 5. Equation (3.18) indicates that the function $f(\vec{x}, t_n)$ depends implicitly on the unknown solution $\phi(\vec{x}, z, t_n)$. In order to compute this apparent contradiction, we apply a fixed-point iteration initialized with the value of $f(\vec{x}, t_{n-1})$ from the previous time step:

$$\hat{f}^{k+1} = -\widehat{\partial_t h} - \mathcal{F} \left[\nabla \phi|_{z=-h}(\hat{f}^k) \cdot \nabla h \right], \quad \hat{f}^0 = \hat{f}(\vec{k}; t_{n-1}).$$

The last product is computed in the physical space:

$$\mathcal{F} \left\{ \nabla \phi|_{z=-h}(\hat{f}^k) \cdot \nabla h \right\} = \mathcal{F} \left[\mathcal{F}^{-1} [\widehat{\nabla \phi|_{z=-h}}(\hat{f}^k)] \cdot \nabla h \right].$$

Simple computations yield

$$\widehat{\nabla \phi|_{z=-h}}(\hat{f}^k) = i\vec{k} \left[\hat{\varphi} \operatorname{sech}(|\vec{k}|H) - \hat{f}^k \frac{\tanh(|\vec{k}|H)}{|\vec{k}|} \right].$$

Our numerical experiments show that this iterative procedure is convergent and the tolerance $\varepsilon := \|\hat{f}^{k+1} - \hat{f}^k\|_\infty \leq 10^{-5}$ is reached after four iterations in average.

The resulting model is only weakly nonlinear since Laplace's equation (3.14) is solved using the Fourier transform in a strip-like domain. Consequently, there is an implicit linearization in the solution procedure. However, the WN model contrary to the CP model not only takes into account some nonlinear effects but can also be efficiently applied to cases with realistic bathymetry. We note that this model is similar to the first order approximation model proposed in [GN07] if in our method we further simplify all expressions by replacing the total water depth H by the undisturbed depth h .

3.3. Time integration. Applying the above Fourier type spectral method to equations (3.12) governing the evolution of the canonical variables η and φ leads to a system of ordinary differential equations, i.e.

$$\Phi_t = \mathcal{A}(t, \Phi), \quad \Phi(t_0) = \Phi_0, \quad \Phi = (\eta, \varphi)^T. \quad (3.20)$$

In order to integrate numerically this system of ODEs we apply an integrating factor method analogous to the one used in [FCKG05, XG09]. This method apparently decreases the stiffness of the system of ODEs and therefore allows for an efficient application of explicit time integration schemes. We start by extracting the linear part of equations (3.20):

$$\Phi_t + \mathcal{L} \cdot \Phi = \mathcal{N}(\Phi), \quad (3.21)$$

where $\mathcal{L} = \begin{pmatrix} 0 & -\frac{\omega^2}{g} \\ g & 0 \end{pmatrix}$ and $\omega = \sqrt{g|\vec{k}| \tanh(|\vec{k}|h_0)}$ is the wave frequency corresponding to the wave number $|\vec{k}|$. For a general bathymetry we choose the constant h_0 to be the mean water depth. (We note that we use the arithmetic average of values provided by the ETOPO1 database in the region under consideration.) The term $\mathcal{N}(\Phi)$ incorporates the remaining nonlinear terms:

$$\mathcal{N}(\Phi) = \begin{pmatrix} \mathcal{F}\{\mathcal{D}_\eta(\varphi)\} - \frac{\omega^2}{g}\hat{\varphi} \\ \mathcal{F}\left\{\frac{1}{2(1+|\nabla\eta|^2)}[\mathcal{D}_\eta(\varphi) + \nabla\varphi \cdot \nabla\eta]^2 - \frac{1}{2}|\nabla\varphi|^2\right\} \end{pmatrix}.$$

The linear terms can be integrated exactly by the following change of variables:

$$\Psi(t) := e^{\mathcal{L}(t-t_0)}\Phi(t), \quad e^{\mathcal{L}(t-t_0)} = \begin{pmatrix} \cos(\omega(t-t_0)) & -\frac{\omega}{g}\sin(\omega(t-t_0)) \\ \frac{g}{\omega}\sin(\omega(t-t_0)) & \cos(\omega(t-t_0)) \end{pmatrix}.$$

Consequently, we solve in practice the following system of ODEs:

$$\Psi_t = e^{\mathcal{L}(t-t_0)}\mathcal{N}(e^{-\mathcal{L}(t-t_0)}\Psi) \equiv \mathcal{B}(t, \Psi), \quad \Psi(t_0) = \Phi_0.$$

This simple modification allows us to take larger CFL numbers, thus improving the overall time stepping performance.

Finally, the system of ODEs is discretized by the standard fourth-order Runge-Kutta (RK4) scheme [HNRW09]:

$$\begin{aligned}\Psi_{n+1} &= \Psi_n + \frac{1}{6}\Delta t(k_1 + 2k_2 + 2k_3 + k_4), \\ k_1 &= \mathcal{B}(t_n, \Psi_n), \\ k_2 &= \mathcal{B}(t_n + \frac{1}{2}\Delta t, \Psi_n + \frac{1}{2}\Delta t k_1), \\ k_3 &= \mathcal{B}(t_n + \frac{1}{2}\Delta t, \Psi_n + \frac{1}{2}\Delta t k_2), \\ k_4 &= \mathcal{B}(t_n + \Delta t, \Psi_n + \Delta t k_3),\end{aligned}\tag{3.22}$$

where the subscript refers to the discrete time instance $\Psi_n := \Psi(t_n)$ and Δt is the discrete time step: $t_{n+1} = t_n + \Delta t$.

In the computations described below, we use a Runge-Kutta (4,5) scheme with an adaptive time step control (cf. [DP80]). However it is not so fundamentally different from the classical RK4 scheme (3.22) described above.

3.4. The BBM-BBM type system. When the long wave approximation is applied to the water wave problem (3.5) – (3.8), one obtains the well-known nonlinear shallow water (or Saint-Venant) equations [dSV71, Sto58, Whi99] which have been extensively used for tsunami simulations [Ima96, TG97, TS98, DKK08, DPD11]. If we go further in the asymptotic expansions, some dispersive effects can be included and generally the resulting system is referred to as Boussinesq system [Bou72, BCS02, MBS03, DD07b, DMS07, DMS09].

In this study we use the Boussinesq system of BBM-BBM type with variable bottom derived in [Mit09]. See also [Per67, Cha07]. The system in dimensional variables can be written as:

$$\begin{aligned}\eta_t + \nabla \cdot ((h_0 + \eta)\vec{u}) + \nabla \cdot \{Ah_0^2[\nabla(\nabla h_0 \cdot \vec{u}) + \nabla h_0 \nabla \cdot \vec{u}] - bh_0^2 \nabla \eta_t\} + \\ A \nabla \cdot (h_0^2 \nabla \zeta_t) + \zeta_t &= 0, \\ \vec{u}_t + g \nabla \eta + \frac{1}{2} \nabla |\vec{u}|^2 + Bgh_0[\nabla(\nabla h \cdot \nabla \eta) + \nabla h_0 \Delta \eta] - dh_0^2 \Delta \vec{u}_t - Bh_0 \nabla \zeta_{tt} &= 0,\end{aligned}\tag{3.23}$$

where A , B , b and d are constants defined as:

$$A = \sqrt{\frac{2}{3}} - \frac{2}{3}, \quad B = 1 - \sqrt{\frac{2}{3}}, \quad b = d = \frac{1}{6}.$$

The variable $\vec{u}(\vec{x}, t)$ denotes the horizontal velocity of the fluid at $z = -h + \sqrt{2/3}(\eta + h)$, and the bathymetry variables $h(\vec{x}, t)$, $h_0(\vec{x})$, $\zeta(\vec{x}, t)$ are defined in Section 2.

We integrate numerically the system (3.23) by using the standard Galerkin/finite element method with $\mathbb{P}1$ elements for the spatial discretization coupled with an explicit, second-order Runge-Kutta method for the temporal discretization (so-called improved Euler scheme) [HNRW09]. A proof that the semidiscrete system is not stiff and thus that the specific RK method is sufficient can be found in [DMS10].

In order to obtain a well-posed problem, we impose homogeneous Dirichlet boundary conditions which absorb partially the wave while reflecting only small amplitude oscillatory waves. Moreover, the specific numerical method appears to converge with optimal rate in the L^2 and L^∞ norms whether we consider structured or unstructured grids. This is contrary to the analogous initial boundary value problems with zero Dirichlet boundary conditions on \vec{u} for the Peregrine system [Per67] where the analogous numerical method

converges with suboptimal orders on structured and unstructured grids. For more information on the properties and the implementation of the numerical method for a BBM-BBM type system we refer to [DMS07, Mit09].

4. NUMERICAL RESULTS

In this section we compare the propagation of a solitary wave when it is used as an initial condition in both the CP and WN models. Moreover, we study the generation and the initial stages of the propagation of the tsunami wave of the July 17, 2006 event. We also present a comparison between the WN, CP and Boussinesq models.

4.1. Solitary wave propagation. Before performing the Java 2006 tsunami generation simulations, we study the propagation of a solitary wave solution to the full water wave problem using the WN and CP models. The initial condition is a solitary wave, computed by using the method presented by Tanaka [Tan86].

Consider the two-dimensional water wave problem in a channel of uniform depth $h_0 = \text{const}$. Since we look for travelling wave solutions, the flow field can be reduced to the steady state by choosing a frame of reference moving with the wave speed c . The introduction of dimensionless variables leads to a single scaling parameter, the Froude number Fr defined as $\text{Fr} := \frac{c}{\sqrt{gh_0}}$. Hereafter, the governing equations are considered in dimensionless form.

The complex velocity potential is classically introduced as $w = \phi + i\psi$, where ψ is the stream function. We choose $\phi = 0$ at the crest and $\psi = 0$ at the bottom. The fluid region is then mapped onto the strip $0 < \psi < 1$, $-\infty < \phi < \infty$ on the plane w with $\psi = 1$ corresponding to the free surface. We introduce the quantity $\Omega = \log \frac{dw}{dz} = \tau - i\theta$, where θ is the angle between the velocity vector and horizontal axis Ox . The real part τ is expressed in terms of the velocity magnitude q as $\tau = \log q$. The boundary conditions to be satisfied are the dynamic condition on the free surface and the bottom impermeability which are expressed as

$$\frac{dq^3}{d\phi} = -\frac{3}{\text{Fr}^2} \sin \theta, \quad \text{on } \psi = 1 \quad \text{and} \quad \theta = 0, \quad \text{on } \psi = 0. \quad (4.1)$$

Consequently, the problem is now transformed into the determination of the complex function Ω , analytic with respect to w within the region of the unit strip $0 < \psi < 1$, decaying at infinity and satisfying the boundary conditions (4.1). By applying Cauchy's integral theorem, one can find the following integral equation on the free surface $\psi = 1$:

$$-\theta(\phi) - \frac{2}{\pi} \int_{-\infty}^{\infty} \frac{\theta(\varphi)}{(\varphi - \phi)^2 + 4} d\varphi = -\frac{1}{\pi} \int_{-\infty}^{\infty} \frac{(\varphi - \phi)\tau(\varphi)}{(\varphi - \phi)^2 + 4} d\varphi + \frac{1}{\pi} \text{p.v.} \int_{-\infty}^{\infty} \frac{\tau(\varphi)}{\varphi - \phi} d\varphi,$$

where $\tau(\phi)$ and $\theta(\phi)$ denote the traces of the corresponding functions on the free surface $\psi = 1$.

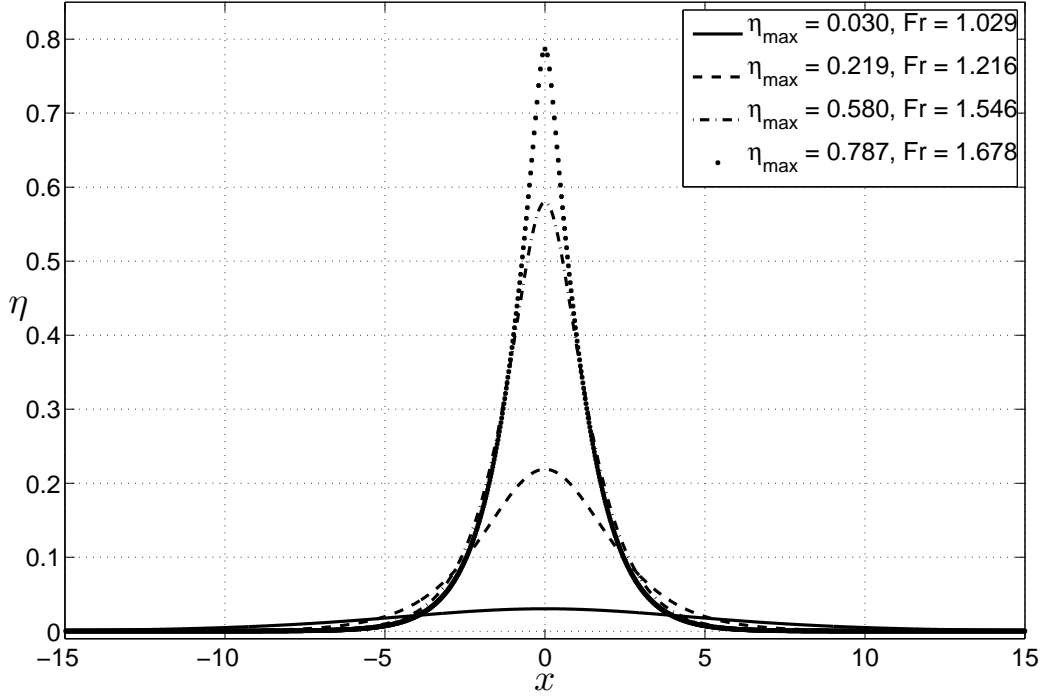


FIGURE 6. Solitary wave solutions of various amplitudes for the full water wave problem. Both x and η have been non-dimensionalized by the depth h_0 .

The integral equation is solved iteratively. The convergence is tested with respect to the Froude number. Several solitary wave solutions computed in this way are plotted on Figure 6 for illustrative purposes.

In order to illustrate the advantages of the proposed WN model over the classical CP solution, we let a solitary wave with amplitude $A/h_0 = 0.1$ propagate up to $T = 80$ (in this section we use dimensionless quantities and time T is non-dimensionalized by $\sqrt{g/h_0}$).

We recall that the classical CP solution of (3.1)–(3.4) corresponding to the initial free surface height $\eta|_{t=0} = \eta_0(x)$ and the velocity potential distribution at the free surface $\varphi|_{t=0} = \varphi_0(x)$, takes the following form:

$$\eta(\vec{x}, t) = \mathcal{F}^{-1} \left\{ \hat{\eta}_0(\vec{k}) \cos(\omega t) + \frac{\omega}{g} \hat{\varphi}_0(\vec{k}) \sin(\omega t) \right\},$$

$$\phi(\vec{x}, z, t) = \mathcal{F}^{-1} \left\{ \left(\hat{\varphi}_0(\vec{k}) \cos(\omega t) - \frac{g}{\omega} \hat{\eta}_0(\vec{k}) \sin(\omega t) \right) (\cosh(|\vec{k}|z) + \tanh(|\vec{k}|h) \sinh(|\vec{k}|z)) \right\},$$

where $\hat{\eta}_0(\vec{k}) = \mathcal{F}\{\eta_0(\vec{x})\}$ and $\hat{\varphi}_0(\vec{k}) = \mathcal{F}\{\varphi_0(\vec{x})\}$ are the Fourier transforms of the initial conditions.

The solution profiles of both models are presented in Figures 7 (a)–(e). One observes that the WN model preserves quite well the shape of the solitary wave while shedding a small dispersive tail behind. The CP solution gradually transforms the initial wave into a

dispersive tail according to the linear nature of equations (3.1)–(3.4). In Figure 7 (f) we present the normalized amplitude error defined as:

$$\epsilon(t) := \frac{|\max_x \{\eta(x, t)\} - A/h_0|}{A/h_0},$$

where $\max_x \{\eta(x, t)\}$ denotes the discrete maximum of the numerical solution and $A/h_0 = 0.1$ is the exact solitary wave amplitude. In both computations a uniform grid of 512 nodes is used. Here, again, we notice a better performance of the WN solver compared to that of the CP solution. This specific experiment shows that the WN model is a better model compared to the CP solution when nonlinear effects must be included for the study of tsunami generation and propagation.

4.2. The July 17, 2006 tsunami generation simulation. The main purpose of this study is to present a novel methodology for tsunami generation problems. This approach is illustrated on the example of the July 17, 2006 Java tsunami since this event is not completely understood yet and there is an available finite fault solution for the presumed generating underwater earthquake.

In this section we show a practical application of the WN method for water waves generated by a moving bottom. Namely, we exploit the bottom motion (2.1) constructed in Section 2.2. The corresponding hydrodynamic problem is solved by the three methods discussed above: the linearized water wave problem (CP), BBM-BBM system and the novel WN model.

The solution given by the WN model and the exact solutions to the linearized Euler equations (3.1) – (3.4) are computed on a uniform grid of 512×512 points. The time step Δt is chosen adaptively according to the RK(4,5) method proposed in [DP80]. The BBM-BBM system is solved on a triangular unstructured grid of 86276 elements. The time integration is performed with the classical RK2 scheme [HNRW09] with time step $\Delta t = 0.5$ s.

Several snapshots of the free surface elevation computed with the WN model are shown in Figures 8 (a) – (f). Analogous contour plots of the solutions of the CP and BBM-BBM models are almost identical and differences cannot be observed within graphical accuracy. Therefore, they are not presented here. The parameters of the bottom motion, bathymetry and computational domain geometry were explained in Section 2.

In this computation, we see a complex process of simultaneous wave evolution together with rupture propagation during approximately 210 s. Namely, the free surface deformed by the rupture of the first subfaults evolves while the rupture continues to propagate along the fault. This kind of fluid/moving bottom interaction cannot be described in the static generation framework, cf. Figure 10.

In order to compare the three models described above we put eight numerical wave gauges at the following locations: six close to the source ((a) $(107.2^\circ, -9.388^\circ)$, (b) $(107.4^\circ, -9.205^\circ)$, (c) $(107.6^\circ, -9.648^\circ)$, (d) $(107.7^\circ, -9.411^\circ)$, (e) $(108.3^\circ, -10.02^\circ)$, (f) $(108.2^\circ, -9.75^\circ)$) and two further away from the source area ((g) $(108^\circ, -10.5^\circ)$, (h) $(108^\circ, -9^\circ)$).

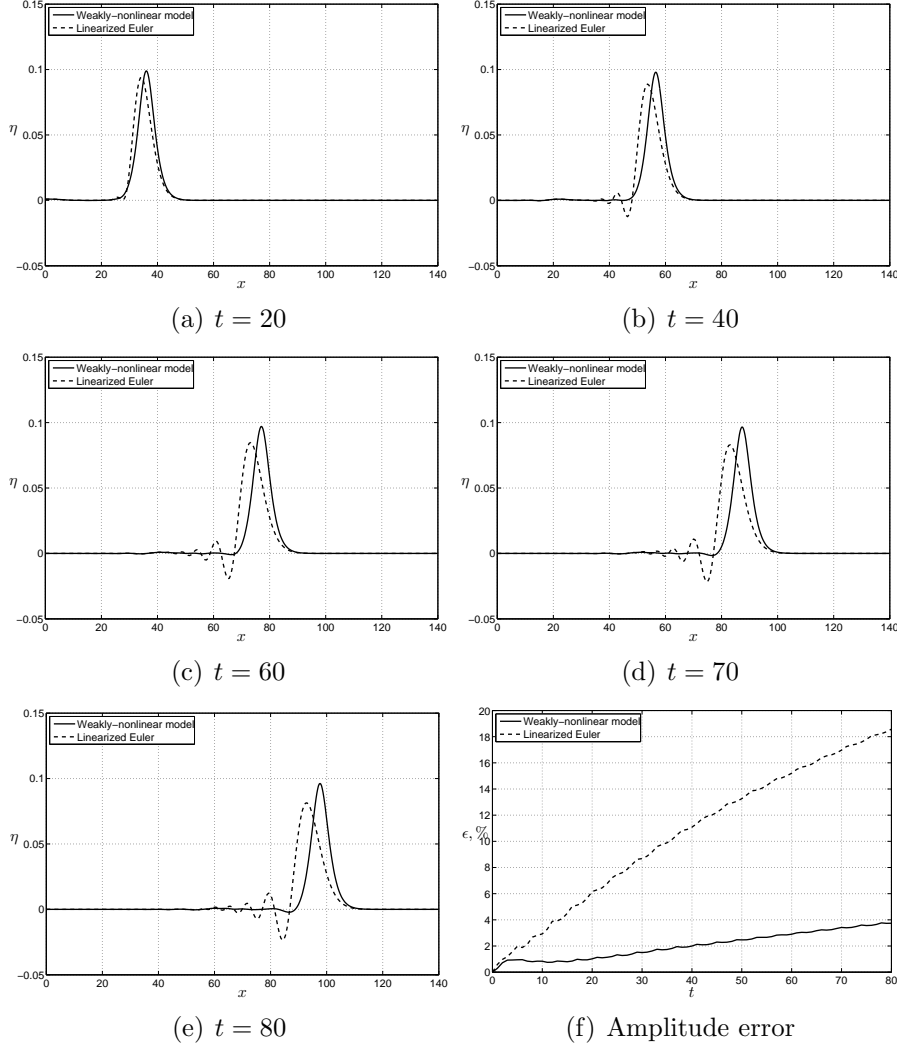


FIGURE 7. Propagation of a solitary wave with the weakly nonlinear method (solid line) and Cauchy-Poisson solution (dashed line). The solitary wave amplitude is $A/h_0 = 0.1$. Space has been scaled by h_0 and time by $\sqrt{g/h_0}$.

The locations of the wave gauges are represented by the symbol \diamond on Figure 9 along with the static sea bed displacement.

The eight wave gauge records are presented in Figures 10 (a)–(h). In order to show the importance of the dynamics of the rupture process, the records obtained from the static approach are also included. The overall agreement among the three dynamic models appears to be satisfactory. We underline that the CP solution is very close to the other solutions despite the fact that the bathymetric features are neglected. We also note that the specific BBM-BBM type system underestimates by a small amount the maximum wave amplitude compared to the WN model. Further numerical tests showed some sensitivity of

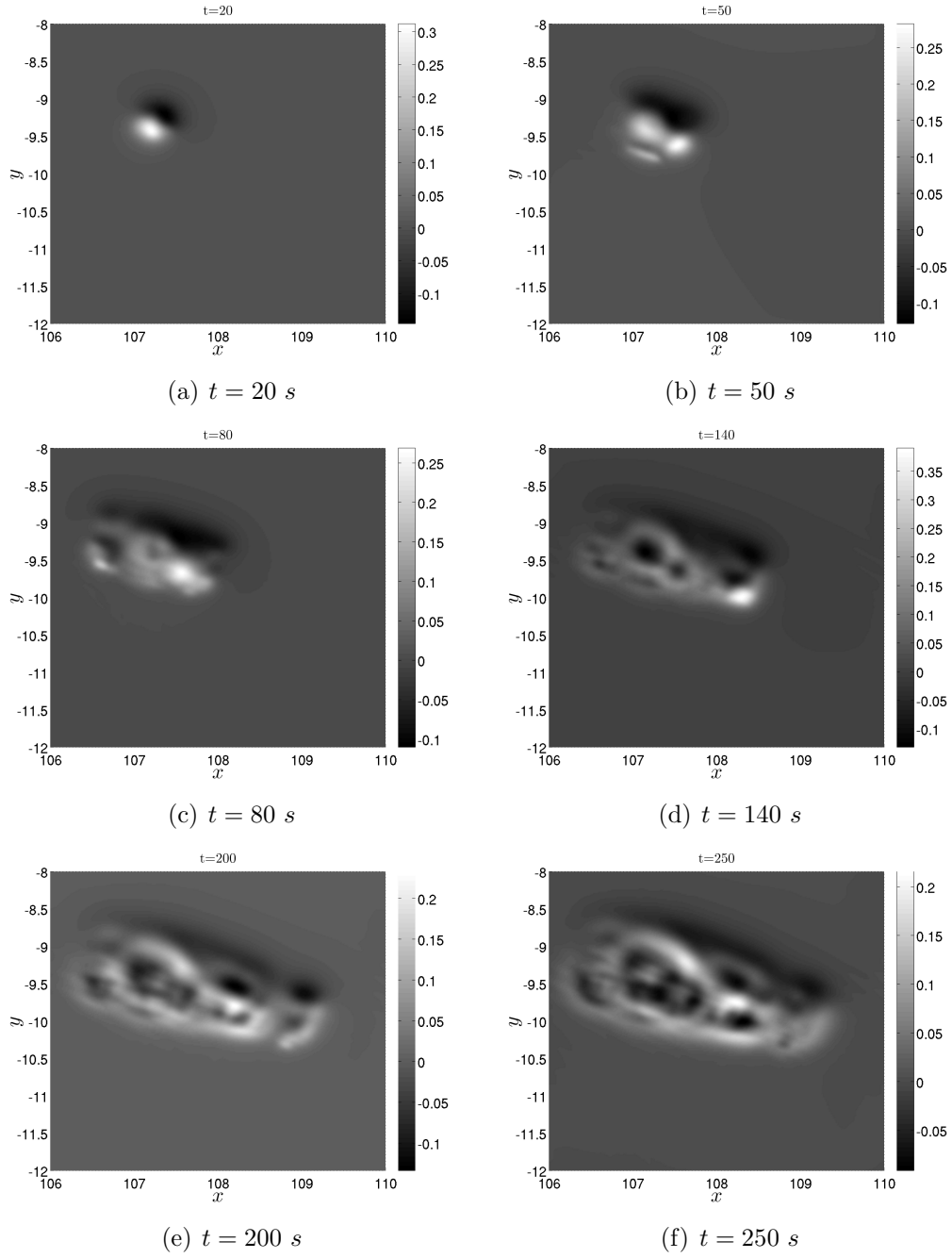


FIGURE 8. Snapshots of the free surface elevation computed with the weakly nonlinear (WN) model. Water waves are generated by dynamic co-seismic bottom displacements (2.1) reconstructed using the corresponding finite fault solution [Ji06].

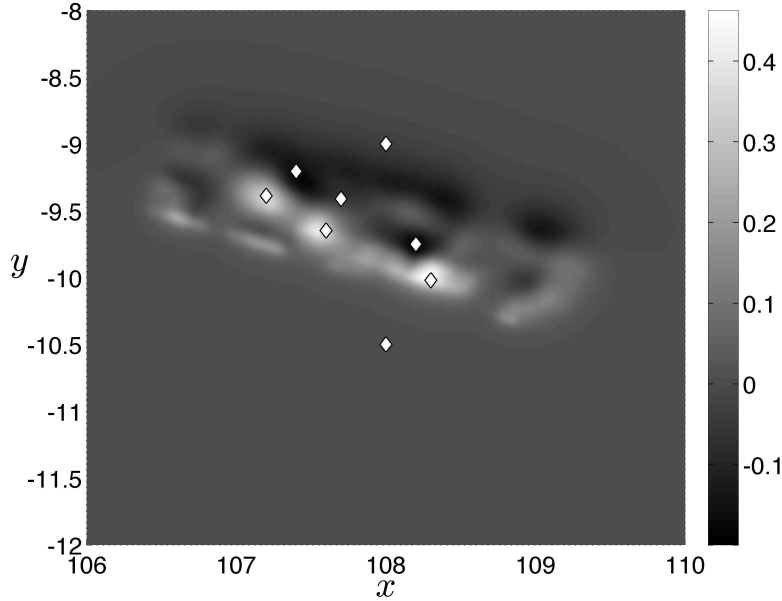


FIGURE 9. Location of the eight numerical wave gauges (indicated by the symbol \diamond) superposed with the static co-seismic bottom displacement.

the BBM-BBM solution to the bottom motion scenario [DD07d]. Namely, we can report, for example, that the exponential scenario led to a slightly larger wave amplitude compared to the other models. As expected, the static approach exhibits differences both in the shape and in the arrival time of the waves. Further away from the source area, the CP solution continues to be accurate. This is due to the fact that nonlinearity is not important during the propagation stage of such small amplitude waves.

5. CONCLUSIONS AND PERSPECTIVES

In the present work we considered an important issue in the modeling of tsunami generation. Namely, a new method for the construction of dynamic co-seismic sea bed displacements was proposed. This method basically relies on two main ingredients:

- the finite fault solution [BLM00, JWH02] gives the slip distribution along the fault
- dynamic sea bed deformation scenarios [Ham73, DDK06, DD07d] allow us to take into account available information of the rupture dynamics

To our knowledge, this reconstruction of the bottom motion is new. All developments presented in this paper are illustrated on the example of the July, 17 2006 Java event.

Along with the bottom motion construction, we discussed three models to solve approximately the corresponding hydrodynamic problem and compute the induced free surface motions. The July 17, 2006 tsunami generation case was computed with three different models and a comparison was performed. We obtained a surprisingly good agreement

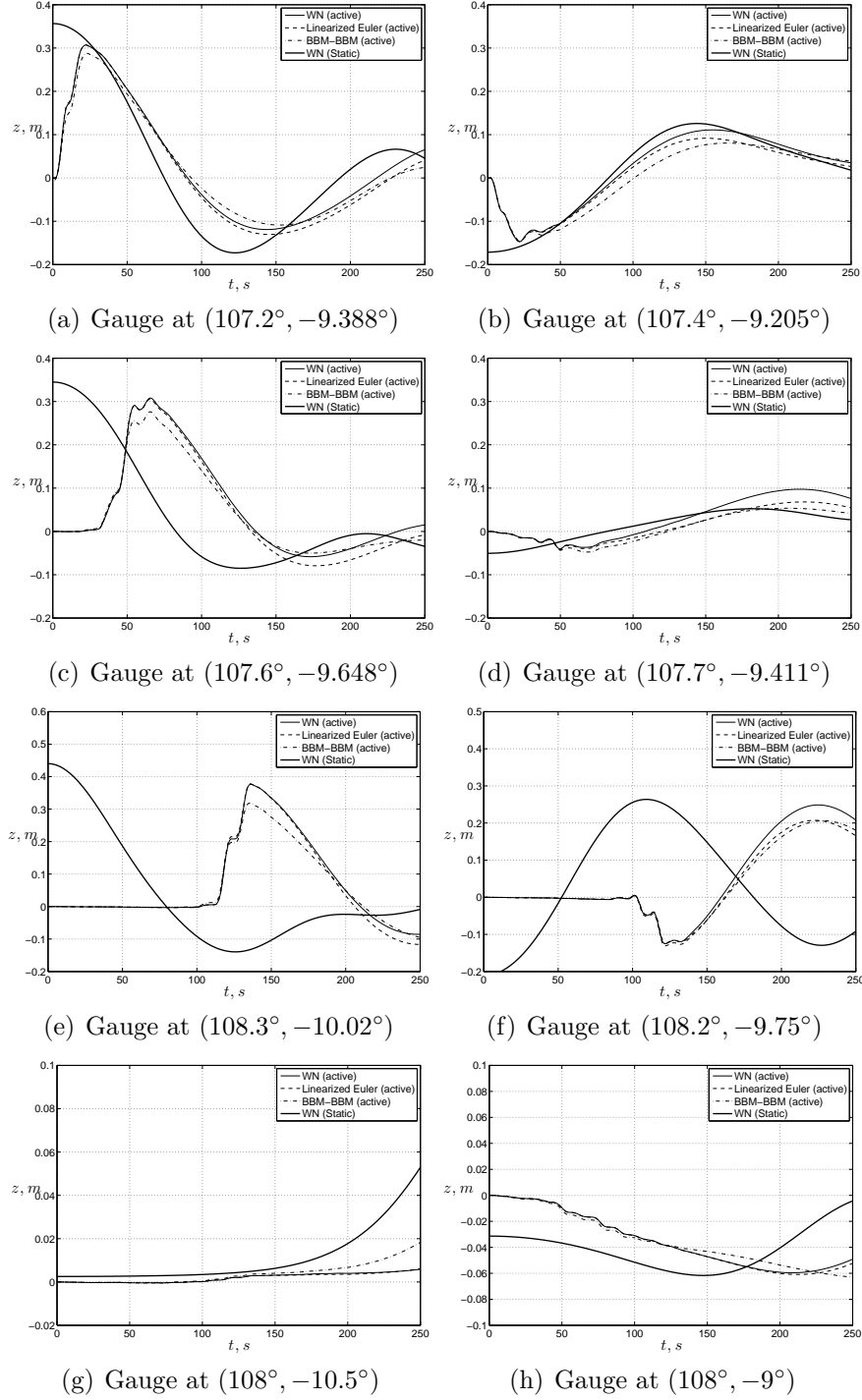


FIGURE 10. Free surface elevation computed numerically with four models at eight wave gauges located approximately at the local extrema of the static bottom displacement. The elevation (vertical axis) is expressed in meters, while the time (horizontal axis) is in seconds. The models 1, 2 and 4 use the dynamic finite-fault rupture (weakly nonlinear model, linearized Euler equations, BBM-BBM model). The third model uses the static approach (weakly nonlinear model).

between the CP solution and the solutions of the other two models. Recall that in the latter the bottom is assumed to be flat. Discrepancies will appear later in time since the bathymetry plays a crucial role in the tsunami propagation.

Taking into account the simplicity and the relatively good accuracy of the new WN approximation to the full water wave problem with time dependent variable bottom, we suggest its use for the computation of the initial stages (≈ 300 s) of the life of a tsunami. The propagation and runup can be computed afterwards by other sophisticated tools [TG97, IYO06, SBT⁺07, DPD11], some of them being already integrated into tsunami warning systems [TGB⁺05, WL08].

However we point out that extreme runup values measured after the July, 17 Java 2006 event [FKM⁺07] deserve additional numerical studies.

APPENDIX A. FINITE FAULT PARAMETERS

Table 3: Subfault parameters given by the finite fault inversion [Ji06].

Latitude, $^{\circ}$	Longitude, $^{\circ}$	Depth, km	Slip, cm	Rake, $^{\circ}$
-10.33298	109.17112	6.81260	5.01844	121.65860
-10.28919	109.04183	6.81260	4.31652	80.93857
-10.24541	108.91254	6.81260	48.94745	85.43047
-10.20162	108.78325	6.81260	3.60585	101.68500
-10.15784	108.65396	6.81260	0.86479	67.04596
-10.11405	108.52467	6.81260	0.96921	99.45411
-10.07027	108.39538	6.81260	0.62447	71.54340
-10.02648	108.26609	6.81260	0.02449	99.44887
-9.98270	108.13680	6.81260	2.71502	119.63240
-9.93891	108.00751	6.81260	0.57000	114.25760
-9.89513	107.87822	6.81260	14.54725	112.71920
-9.85134	107.74893	6.81260	31.66312	107.26750
-9.80756	107.61964	6.81260	2.74176	85.79224
-9.76377	107.49035	6.81260	3.35868	78.97166
-9.71999	107.36105	6.81260	67.95367	64.89334
-9.67620	107.23177	6.81260	62.33453	65.43832
-9.63242	107.10248	6.81260	35.33318	66.90181
-9.58863	106.97318	6.81260	1.75233	101.93900
-9.54485	106.84389	6.81260	40.63542	81.77631
-9.50106	106.71461	6.81260	84.20831	68.95723
-9.45728	106.58531	6.81260	25.12981	66.62241
-10.24093	109.20313	8.78887	0.68254	88.79068
-10.19714	109.07384	8.78887	30.70282	97.90491
-10.15336	108.94455	8.78887	76.07102	99.93182
-10.10957	108.81525	8.78887	0.56201	79.59160
-10.06579	108.68597	8.78887	0.95023	114.32920

Continued on the next page

Latitude, °	Longitude, °	Depth, <i>km</i>	Slip, <i>cm</i>	Rake, °
-10.02201	108.55668	8.78887	64.78191	121.81120
-9.97822	108.42738	8.78887	81.31910	105.21240
-9.93443	108.29810	8.78887	137.60680	121.72020
-9.89065	108.16881	8.78887	85.81732	88.13734
-9.84686	108.03951	8.78887	30.61069	80.38488
-9.80308	107.91022	8.78887	60.08308	113.75000
-9.75929	107.78094	8.78887	46.98381	96.25403
-9.71551	107.65164	8.78887	21.69421	80.82516
-9.67173	107.52235	8.78887	11.01957	112.63110
-9.62794	107.39307	8.78887	27.85978	75.88463
-9.58416	107.26377	8.78887	5.96505	77.66200
-9.54037	107.13448	8.78887	3.85634	83.57522
-9.49658	107.00520	8.78887	3.23158	113.73070
-9.45280	106.87590	8.78887	29.89915	116.10890
-9.40902	106.74661	8.78887	65.25044	72.60931
-9.36523	106.61732	8.78887	19.62932	65.99193
-10.14888	109.23514	10.76514	20.60663	124.43320
-10.10510	109.10584	10.76514	69.91051	122.64720
-10.06131	108.97655	10.76514	63.10052	99.23547
-10.01753	108.84727	10.76514	0.63700	74.09311
-9.97374	108.71797	10.76514	1.02761	117.53560
-9.92996	108.58868	10.76514	85.54328	123.64950
-9.88617	108.45940	10.76514	167.18620	104.56840
-9.84239	108.33010	10.76514	202.60880	122.12460
-9.79860	108.20081	10.76514	144.76970	81.50333
-9.75482	108.07152	10.76514	53.97212	72.84430
-9.71103	107.94223	10.76514	79.21021	98.66053
-9.66725	107.81294	10.76514	82.95619	80.81979
-9.62346	107.68365	10.76514	119.13390	74.36982
-9.57968	107.55436	10.76514	95.90159	116.24710
-9.53589	107.42507	10.76514	36.94965	102.32060
-9.49211	107.29578	10.76514	0.28681	81.49704
-9.44832	107.16649	10.76514	8.06018	98.40840
-9.40454	107.03720	10.76514	3.02927	116.89820
-9.36075	106.90791	10.76514	10.73559	74.60908
-9.31697	106.77862	10.76514	57.94233	75.39254
-9.27318	106.64933	10.76514	60.97223	64.77096
-10.05684	109.26714	12.74141	21.97392	121.10740
-10.01305	109.13785	12.74141	74.47045	119.75060
-9.96927	109.00856	12.74141	17.25334	124.09410
-9.92548	108.87927	12.74141	14.38904	87.41515
-9.88170	108.74998	12.74141	3.03040	106.36440
-9.83791	108.62069	12.74141	8.97587	101.53580
-9.79413	108.49140	12.74141	114.85160	115.94270

Continued on the next page

Latitude, °	Longitude, °	Depth, <i>km</i>	Slip, <i>cm</i>	Rake, °
-9.75034	108.36211	12.74141	91.90382	115.95240
-9.70656	108.23282	12.74141	64.72478	100.08050
-9.66277	108.10353	12.74141	17.30368	123.06770
-9.61899	107.97424	12.74141	57.09099	68.20686
-9.57520	107.84495	12.74141	64.81193	79.84035
-9.53142	107.71566	12.74141	131.04410	76.45924
-9.48763	107.58636	12.74141	112.11020	99.51801
-9.44385	107.45708	12.74141	60.23628	97.77266
-9.40006	107.32778	12.74141	126.96870	80.27277
-9.35628	107.19849	12.74141	63.39000	65.00801
-9.31249	107.06921	12.74141	0.52621	94.79313
-9.26871	106.93991	12.74141	1.52171	66.78681
-9.22492	106.81062	12.74141	10.96743	81.94861
-9.18114	106.68134	12.74141	2.38062	123.04830
-9.96479	109.29915	14.71768	22.40949	123.90350
-9.92100	109.16986	14.71768	48.62879	115.45630
-9.87722	109.04057	14.71768	5.99559	83.81007
-9.83343	108.91128	14.71768	7.22945	123.80940
-9.78965	108.78199	14.71768	0.10031	93.40998
-9.74586	108.65269	14.71768	0.36991	69.37087
-9.70208	108.52341	14.71768	104.18760	123.83230
-9.65829	108.39411	14.71768	46.12533	95.97049
-9.61451	108.26482	14.71768	0.28679	89.56866
-9.57072	108.13554	14.71768	2.06597	80.14312
-9.52694	108.00624	14.71768	30.55070	66.23147
-9.48315	107.87695	14.71768	73.72994	87.91253
-9.43937	107.74767	14.71768	112.90700	92.28181
-9.39558	107.61837	14.71768	74.73608	86.51558
-9.35180	107.48908	14.71768	121.73820	64.68654
-9.30801	107.35979	14.71768	231.20940	65.50779
-9.26423	107.23050	14.71768	96.55727	87.01543
-9.22044	107.10121	14.71768	28.29534	122.55670
-9.17666	106.97192	14.71768	0.84110	70.21989
-9.13287	106.84263	14.71768	7.99213	87.51706
-9.08909	106.71334	14.71768	1.33281	96.33266
-9.87274	109.33115	16.69394	43.31154	121.79150
-9.82896	109.20187	16.69394	87.17052	124.49750
-9.78517	109.07257	16.69394	61.47630	87.10537
-9.74139	108.94328	16.69394	31.53286	70.58137
-9.69760	108.81400	16.69394	0.70628	65.17896
-9.65382	108.68470	16.69394	5.74160	87.70702
-9.61003	108.55541	16.69394	93.47714	107.32000
-9.56625	108.42612	16.69394	93.55753	85.39201
-9.52246	108.29683	16.69394	47.25525	74.24297

Continued on the next page

Latitude, °	Longitude, °	Depth, <i>km</i>	Slip, <i>cm</i>	Rake, °
-9.47868	108.16754	16.69394	24.65230	124.20110
-9.43489	108.03825	16.69394	35.63115	71.78733
-9.39111	107.90896	16.69394	25.11757	75.27779
-9.34732	107.77967	16.69394	68.15302	107.42980
-9.30354	107.65038	16.69394	24.66007	112.77880
-9.25975	107.52109	16.69394	0.50688	79.86887
-9.21597	107.39180	16.69394	119.92850	75.03103
-9.17218	107.26250	16.69394	77.08335	110.83160
-9.12840	107.13322	16.69394	31.65430	123.83060
-9.08461	107.00393	16.69394	11.42768	66.47282
-9.04083	106.87463	16.69394	33.80650	115.65650
-8.99704	106.74535	16.69394	39.47481	65.15574
-9.78069	109.36316	18.67021	35.42621	111.95830
-9.73691	109.23387	18.67021	103.05030	124.62650
-9.69312	109.10458	18.67021	101.38220	122.70620
-9.64934	108.97529	18.67021	76.76701	68.20042
-9.60556	108.84600	18.67021	10.71945	77.79713
-9.56177	108.71671	18.67021	1.32449	100.72950
-9.51799	108.58742	18.67021	37.46857	124.59330
-9.47420	108.45813	18.67021	118.99580	100.38000
-9.43042	108.32883	18.67021	79.62616	91.56905
-9.38663	108.19955	18.67021	97.61735	109.86430
-9.34285	108.07026	18.67021	87.67753	87.57239
-9.29906	107.94096	18.67021	15.14859	64.75201
-9.25528	107.81168	18.67021	82.60960	71.66805
-9.21149	107.68239	18.67021	66.06397	98.55843
-9.16771	107.55309	18.67021	0.43085	67.81042
-9.12392	107.42381	18.67021	35.30429	124.04570
-9.08014	107.29452	18.67021	59.17323	124.55130
-9.03635	107.16522	18.67021	15.23214	66.82615
-8.99257	107.03593	18.67021	28.10358	76.08198
-8.94878	106.90664	18.67021	48.09923	124.24450
-8.90500	106.77735	18.67021	42.38682	124.42850

APPENDIX B. ZAKHAROV'S FORMULATION OF THE WATER WAVE PROBLEM

In this appendix we recast the governing equations (3.5) – (3.8) of the water wave problem in a more compact and mathematically more convenient form [Zak68, CS93].

Using the definition of the normal velocity (3.11), it is straightforward to rewrite the kinematic free surface condition (3.6):

$$\partial_t \eta - \mathcal{D}_\eta(\varphi) = 0,$$

where φ is the trace of the velocity potential at the free surface (3.10).

The time derivative and the horizontal gradient of the velocity potential trace on the free surface can be computed:

$$\partial_t \varphi = \partial_t \phi + \partial_t \eta \partial_z \phi|_{z=\eta} = \partial_t \phi + \mathcal{D}_\eta(\varphi) \partial_z \phi|_{z=\eta}, \quad (\text{B.1})$$

and similarly one can compute the horizontal gradient:

$$\nabla \varphi = \nabla \phi|_{z=\eta} + \nabla \eta \partial_z \phi|_{z=\eta}. \quad (\text{B.2})$$

In order to close the system, we have to express all derivatives of the potential ϕ computed at the free surface, in terms of φ , η and $\mathcal{D}_\eta(\varphi)$.

From the definition of the normal velocity (3.11) and the D2N operator one readily obtains:

$$\nabla \phi|_{z=\eta} \cdot \nabla \eta = \partial_z \phi|_{z=\eta} - \mathcal{D}_\eta(\varphi). \quad (\text{B.3})$$

Substituting the last identity into (B.2) multiplied by $\nabla \eta$, leads to the following expression:

$$\partial_z \phi|_{z=\eta} = \frac{\mathcal{D}_\eta(\varphi) + \nabla \varphi \cdot \nabla \eta}{1 + |\nabla \eta|^2}. \quad (\text{B.4})$$

Now we have all elements to find the horizontal derivatives of the velocity potential:

$$\nabla \phi|_{z=\eta} = \nabla \varphi - \nabla \eta \partial_z \phi|_{z=\eta} = \frac{(1 + |\nabla \eta|^2) \nabla \varphi - \mathcal{D}_\eta(\varphi) \nabla \eta - (\nabla \varphi \cdot \nabla \eta) \nabla \eta}{1 + |\nabla \eta|^2}. \quad (\text{B.5})$$

In order to rewrite Bernoulli condition (3.7) in new variables, we make the following observation (using (B.2) and (B.3)):

$$\begin{aligned} \frac{1}{2} |\nabla \phi|^2 + \frac{1}{2} (\partial_z \phi)^2 &= \frac{1}{2} \nabla \phi \cdot \nabla \phi + \frac{1}{2} \partial_z \phi \partial_z \phi = \\ &= \frac{1}{2} \nabla \phi \cdot (\nabla \varphi - \partial_z \phi \nabla \eta) + \frac{1}{2} \partial_z \phi (\mathcal{D}_\eta(\varphi) + \nabla \phi \cdot \nabla \eta) = \frac{1}{2} \nabla \phi \cdot \nabla \varphi + \frac{1}{2} \mathcal{D}_\eta(\varphi) \partial_z \phi, \quad z = \eta. \end{aligned}$$

Taking into account this observation and expression (B.1) for the time derivative of φ , the dynamic condition takes this equivalent form:

$$\partial_t \varphi + g\eta + \frac{1}{2} \nabla \phi \cdot \nabla \varphi - \frac{1}{2} \mathcal{D}_\eta(\varphi) \partial_z \phi = 0, \quad z = \eta.$$

After substituting expressions (B.4), (B.5) into the last equation and summarizing all the developments made above, we get the following set of dynamic equations equivalent to the complete water wave problem (3.5) – (3.8):

$$\begin{aligned} \partial_t \eta - \mathcal{D}_\eta(\varphi) &= 0, \\ \partial_t \varphi + \frac{1}{2} |\nabla \varphi|^2 + g\eta - \frac{1}{2(1+|\nabla \eta|^2)} [\mathcal{D}_\eta(\varphi) + \nabla \varphi \cdot \nabla \eta]^2 &= 0. \end{aligned}$$

APPENDIX C. RELATIONS BETWEEN ELASTIC CONSTANTS

In the classical elasticity theory, coefficients in Lamé equations (governing the displacements field in an elastic solid), can be expressed in terms of various sets of physical parameters [Lov44, SS46]. The purpose of this Appendix is to recall some relations between them.

Lamé coefficients λ and μ can be defined in terms of the Young's modulus E (having the dimension of the pressure $[Pa]$) and Poisson's ratio ν (dimensionless coefficient $0 < \nu < 1/2$):

$$\lambda = \frac{E\nu}{(1+\nu)(1-2\nu)}, \quad \mu = \frac{E}{2(1+\nu)},$$

and inversely:

$$E = \frac{(3\lambda + 2\mu)\mu}{\lambda + \mu}, \quad \nu = \frac{\lambda}{2(\lambda + \mu)}.$$

The celerities of P and S waves have the following expressions in terms of Lamé coefficients:

$$c_p = \sqrt{\frac{\lambda + 2\mu}{\rho}}, \quad c_s = \sqrt{\frac{\mu}{\rho}},$$

where ρ is the density of elastic medium. These relations yield

$$\mu = \rho c_s^2, \quad \lambda = \rho c_p^2 - 2\mu.$$

ACKNOWLEDGEMENT

D. Dutykh acknowledges the support from French Agence Nationale de la Recherche, project MathOcean (Grant ANR-08-BLAN-0301-01). F. Dias and D. Dutykh acknowledge the support of the Ulysses Program of the French Ministry of Foreign Affairs under the project 23725ZA.

Special thanks go to Professor Costas Synolakis whose work on tsunami waves has been the source of our inspiration. Finally we would like to thank Professor Didier Clamond for very helpful discussions on the numerical simulation of water waves.

REFERENCES

- [AKLV06] C. J. Ammon, H. Kanamori, T. Lay, and A. A. Velasco. The 17 July 2006 Java tsunami earthquake. *Geophysical Research Letters*, 33:L24308, 2006. [2](#), [4](#)
- [Bas06] R. Basher. Global Early Warning Systems for Natural Hazards: Systematic and People-Centred. *Philosophical Transactions: Mathematical, Physical and Engineering Sciences*, 364(1845):2167–2182, 2006. [1](#)
- [BCS02] J. L. Bona, M. Chen, and J.-C. Saut. Boussinesq equations and other systems for small-amplitude long waves in nonlinear dispersive media. I: Derivation and linear theory. *Journal of Nonlinear Science*, 12:283–318, 2002. [14](#)
- [BLM00] C. Bassin, G. Laske, and G. Masters. The Current Limits of Resolution for Surface Wave Tomography in North America. *EOS Trans AGU*, 81:F897, 2000. [2](#), [4](#), [20](#)
- [Bou72] J. Boussinesq. Théorie des ondes et des remous qui se propagent le long d'un canal rectangulaire horizontal, en communiquant au liquide contenu dans ce canal des vitesses sensiblement pareilles de la surface au fond. *J. Math. Pures Appl.*, 17:55–108, 1872. [14](#)
- [Cau27] A.-L. Cauchy. Mémoire sur la théorie de la propagation des ondes à la surface d'un fluide pesant d'une profondeur indéfinie. *Mém. Présentés Divers Savans Acad. R. Sci. Inst. France*, 1:3–312, 1827. [8](#)
- [Cha07] F. Chazel. Influence of bottom topography on long water waves. *M2AN*, 41:771–799, 2007. [14](#)
- [CM85] R. R. Coifman and Y. Meyer. Nonlinear harmonic analysis and analytic dependence. *Pseudo-differential Operators and Applications*, 43:71–78, 1985. [11](#)

- [CS93] W. Craig and C. Sulem. Numerical simulation of gravity waves. *J. Comput. Phys.*, 108:73–83, 1993. [11](#), [25](#)
- [CSS92] W. Craig, C. Sulem, and P.-L. Sulem. Nonlinear modulation of gravity waves: a rigorous approach. *Nonlinearity*, 5(2):497–522, 1992. [11](#)
- [CT65] J. W. Cooley and J. W. Tukey. An algorithm for the machine calculation of complex Fourier series. *Math. Comput.*, 19:297–301, 1965. [11](#)
- [DB06] F. Dias and T. J. Bridges. The numerical computation of freely propagating time-dependent irrotational water waves. *Fluid Dynamics Research*, 38:803–830, 2006. [10](#)
- [DD07a] F. Dias and D. Dutykh. *Dynamics of tsunami waves*, chapter Dynamics o, pages 35–60. Springer, 2007. [4](#)
- [DD07b] D. Dutykh and F. Dias. Dissipative Boussinesq equations. *C. R. Mecanique*, 335:559–583, 2007. [14](#)
- [DD07c] D. Dutykh and F. Dias. Viscous potential free-surface flows in a fluid layer of finite depth. *C. R. Acad. Sci. Paris, Ser. I*, 345:113–118, 2007. [10](#)
- [DD07d] D. Dutykh and F. Dias. Water waves generated by a moving bottom. In Anjan Kundu, editor, *Tsunami and Nonlinear waves*, pages 65–96. Springer Verlag (Geo Sc.), 2007. [1](#), [2](#), [4](#), [5](#), [7](#), [8](#), [9](#), [10](#), [18](#), [20](#)
- [DD09] D. Dutykh and F. Dias. Tsunami generation by dynamic displacement of sea bed due to dip-slip faulting. *Mathematics and Computers in Simulation*, 80(4):837–848, 2009. [1](#), [2](#)
- [DD10] D. Dutykh and F. Dias. Influence of sedimentary layering on tsunami generation. *Computer Methods in Applied Mechanics and Engineering*, 199(21-22):1268–1275, 2010. [1](#)
- [DDK06] D. Dutykh, F. Dias, and Y. Kervella. Linear theory of wave generation by a moving bottom. *C. R. Acad. Sci. Paris, Ser. I*, 343:499–504, 2006. [2](#), [7](#), [20](#)
- [DDZ08] F. Dias, A. I. Dyachenko, and V. E. Zakharov. Theory of weakly damped free-surface flows: a new formulation based on potential flow solutions. *Physics Letters A*, 372:1297–1302, 2008. [10](#)
- [DKK08] A. I. Delis, M. Kazolea, and N. A. Kampanis. A robust high-resolution finite volume scheme for the simulation of long waves over complex domains. *Int. J. Numer. Meth. Fluids*, 56:419–452, 2008. [14](#)
- [DMS07] V. A. Dougalis, D. E. Mitsotakis, and J.-C. Saut. On some Boussinesq systems in two space dimensions: Theory and numerical analysis. *Math. Model. Num. Anal.*, 41(5):254–825, 2007. [14](#), [15](#)
- [DMS09] V. A. Dougalis, D. E. Mitsotakis, and J.-C. Saut. On initial-boundary value problems for a Boussinesq system of BBM-BBM type in a plane domain. *Discrete Contin. Dyn. Syst.*, 23(4):1191–1204, 2009. [14](#)
- [DMS10] V. A. Dougalis, D. E. Mitsotakis, and J.-C. Saut. Initial-boundary-value problems for Boussinesq systems of Bona-Smith type on a plane domain: theory and numerical analysis. *J. Sci. Comput.*, 44:109–135, 2010. [14](#)
- [DP80] J. R. Dormand and P. J. Prince. A family of embedded Runge-Kutta formulae. *J. Comp. Appl. Math.*, 6:19–26, 1980. [14](#), [17](#)
- [DPD11] D. Dutykh, R. Poncet, and F. Dias. The VOLNA code for the numerical modeling of tsunami waves: Generation, propagation and inundation. *Eur. J. Mech. B/Fluids*, 30(6):598–615, 2011. [1](#), [2](#), [14](#), [22](#)
- [dSV71] A. J. C. de Saint-Venant. Théorie du mouvement non-permanent des eaux, avec application aux crues des rivières et à l’introduction des marées dans leur lit. *C. R. Acad. Sc. Paris*, 73:147–154, 1871. [14](#)
- [Dut07] D. Dutykh. *Mathematical modelling of tsunami waves*. Ph.d. thesis, École Normale Supérieure de Cachan, December 2007. [1](#), [2](#), [4](#), [10](#)
- [Dut09a] D. Dutykh. Group and phase velocities in the free-surface visco-potential flow: new kind of boundary layer induced instability. *Physics Letters A*, 373:3212–3216, 2009. [10](#)

- [Dut09b] D. Dutykh. Visco-potential free-surface flows and long wave modelling. *Eur. J. Mech. B/Fluids*, 28:430–443, 2009. [10](#)
- [FCKG05] D. Fructus, D. Clamond, O. Kristiansen, and J. Grue. An efficient model for three-dimensional surface wave simulations. Part I: Free space problems. *J. Comput. Phys.*, 205:665–685, 2005. [11](#), [13](#)
- [FJ05] M. Frigo and S. G. Johnson. The Design and Implementation of FFTW3. *Proceedings of the IEEE*, 93(2):216–231, 2005. [11](#)
- [FKM⁺07] H. M. Fritz, W. Kongko, A. Moore, B. McAdoo, J. Goff, C. Harbitz, B. Uslu, N. Kalligeris, D. Suteja, K. Kalsum, V. V. Titov, A. Gusman, H. Latief, E. Santoso, S. Sujoko, D. Djulkarnaen, H. Sunendar, and C. Synolakis. Extreme runup from the 17 July 2006 Java tsunami. *Geophys. Res. Lett.*, 34:L12602, 2007. [4](#), [22](#)
- [GBM⁺05] F. I. González, E. N. Bernard, C. Meinig, M. C. Eble, H. O. Mofjeld, and S. Stalin. The NTHMP tsunameter network. *Natural Hazards*, 35:25–39, 2005. [1](#)
- [GN07] P. Guyenne and D. P. Nicholls. A high-order spectral method for nonlinear water waves over moving bottom topography. *SIAM J. Sci. Comput.*, 30(1):81–101, 2007. [13](#)
- [Ham72] J. L. Hammack. *Tsunamis - A Model of Their Generation and Propagation*. PhD thesis, California Institute of Technology, 1972. [7](#), [8](#)
- [Ham73] J. Hammack. A note on tsunamis: their generation and propagation in an ocean of uniform depth. *J. Fluid Mech.*, 60:769–799, 1973. [1](#), [7](#), [8](#), [9](#), [20](#)
- [HNrW09] E. Hairer, S. P. Nørsett, and G. Wanner. *Solving ordinary differential equations: Nonstiff problems*. Springer, 2009. [14](#), [17](#)
- [IAK⁺07] M. Ioualalen, J. Asavanant, N. Kaewbanjak, S. T. Grilli, J. T. Kirby, and P. Watts. Modeling the 26 December 2004 Indian Ocean tsunami: Case study of impact in Thailand. *Journal of Geophysical Research*, 112:C07024, 2007. [2](#)
- [Ima96] F. Imamura. *Long-wave runup models*, chapter Simulation, pages 231–241. World Scientific, 1996. [1](#), [14](#)
- [IYO06] F. Imamura, A. C. Yalciner, and G. Ozyurt. *Tsunami modelling manual*, April 2006. [22](#)
- [Ji06] C. Ji. Preliminary Result of the 2006 July 17 Magnitude 7.7 - South of Java, Indonesia Earthquake. Technical report, USGS, 2006. [4](#), [5](#), [6](#), [7](#), [19](#), [22](#)
- [JWH02] C. Ji, D. J. Wald, and D. V. Helmberger. Source description of the 1999 Hector Mine, California earthquake; Part I: Wavelet domain inversion theory and resolution analysis. *Bull. Seism. Soc. Am.*, 92(4):1192–1207, 2002. [2](#), [4](#), [20](#)
- [Kaj63] K. Kajiura. The leading wave of tsunami. *Bull. Earthquake Res. Inst., Tokyo Univ.*, 41:535–571, 1963. [1](#), [7](#)
- [KDD07] Y. Kervella, D. Dutykh, and F. Dias. Comparison between three-dimensional linear and nonlinear tsunami generation models. *Theor. Comput. Fluid Dyn.*, 21:245–269, 2007. [7](#), [9](#), [10](#)
- [Lam32] H. Lamb. *Hydrodynamics*. Cambridge University Press, 1932. [10](#)
- [Lov44] A. E. H. Love. *A treatise on the mathematical theory of elasticity*. Dover Publications, New York, 1944. [26](#)
- [MBS03] P. A. Madsen, H. B. Bingham, and H. A. Schaffer. Boussinesq-type formulations for fully nonlinear and extremely dispersive water waves: derivation and analysis. *Proc. R. Soc. Lond. A*, 459:1075–1104, 2003. [14](#)
- [Mei94] C. C. Mei. *The applied dynamics of ocean surface waves*. World Scientific, 1994. [10](#)
- [Min36] R. D. Mindlin. Force at a point in the interior of a semi-infinite medium. *Physics*, 7:195–202, 1936. [4](#)
- [Mit09] D. E. Mitsotakis. Boussinesq systems in two space dimensions over a variable bottom for the generation and propagation of tsunami waves. *Math. Comp. Simul.*, 80:860–873, 2009. [14](#), [15](#)
- [MS67] L. Mansinha and D. E. Smylie. Effect of earthquakes on the Chandler wobble and the secular polar shift. *J. Geophys. Res.*, 72:4731–4743, 1967. [2](#), [4](#)

- [MS71] L. Mansinha and D. E. Smylie. The displacement fields of inclined faults. *Bull. Seism. Soc. Am.*, 61:1433–1440, 1971. [2](#), [4](#)
- [Oka85] Y. Okada. Surface deformation due to shear and tensile faults in a half-space. *Bull. Seism. Soc. Am.*, 75:1135–1154, 1985. [1](#), [2](#), [4](#)
- [Oka92] Y. Okada. Internal deformation due to shear and tensile faults in a half-space. *Bull. Seism. Soc. Am.*, 82:1018–1040, 1992. [1](#), [2](#), [4](#)
- [OTM01] T. Ohmachi, H. Tsukiyama, and H. Matsumoto. Simulation of tsunami induced by dynamic displacement of seabed due to seismic faulting. *Bull. Seism. Soc. Am.*, 91:1898–1909, 2001. [2](#)
- [Ozg06] A. Ozgun Konca. Preliminary Result 06/07/17 (Mw 7.9) , Southern Java Earthquake. Technical report, USGS, 2006. [4](#)
- [Per67] D. H. Peregrine. Long waves on a beach. *J. Fluid Mech.*, 27:815–827, 1967. [14](#)
- [Pre65] F. Press. Displacements, strains and tilts at tele-seismic distances. *J. Geophys. Res.*, 70:2395–2412, 1965. [4](#)
- [RLF⁺08] A. B. Rabinovich, L. I. Lobkovsky, I. V. Fine, R. E. Thomson, T. N. Ivelskaya, and E. A. Kulikov. Near-source observations and modeling of the Kuril Islands tsunamis of 15 November 2006 and 13 January 2007. *Adv. Geosci.*, 14:105–116, 2008. [2](#)
- [SB06] C. E. Synolakis and E. N. Bernard. Tsunami science before and beyond Boxing Day 2004. *Phil. Trans. R. Soc. A*, 364:2231–2265, 2006. [1](#), [2](#)
- [SBT⁺07] C. E. Synolakis, E. N. Bernard, V. V. Titov, U. Kanoglu, and F. I. Gonzalez. Standards, criteria, and procedures for NOAA evaluation of tsunami numerical models. Technical report, NOAA/Pacific Marine Environmental Laboratory, 2007. [22](#)
- [SF09] T. Saito and T. Furumura. Three-dimensional tsunami generation simulation due to sea-bottom deformation and its interpretation based on the linear theory. *Geophys. J. Int.*, 178:877–888, 2009. [2](#), [9](#), [10](#)
- [SS46] I. S. Sokolnikoff and R. D. Specht. *Mathematical theory of elasticity*. McGraw-Hill, New York, 1946. [26](#)
- [Sto58] J. J. Stoker. *Water waves, the mathematical theory with applications*. Wiley, 1958. [10](#), [14](#)
- [Syn05] C. Synolakis. India must cooperate on tsunami warning system. *Nature*, 434:17–18, 2005. [1](#)
- [Tan86] M. Tanaka. The stability of solitary waves. *Phys. Fluids*, 29(3):650–655, 1986. [15](#)
- [TDS07] P. Tkalich, M. H. Dao, and C. E. Soon. Tsunami propagation modeling and forecasting for early warning system. *Journal of Earthquake and Tsunami*, 1(1):87–98, 2007. [1](#)
- [TG97] V. V. Titov and F. I. González. Implementation and testing of the method of splitting tsunami (MOST) model. Technical Report ERL PMEL-112, Pacific Marine Environmental Laboratory, NOAA, 1997. [1](#), [14](#), [22](#)
- [TGB⁺05] V. V. Titov, F. I. Gonzalez, E. N. Bernard, M. C. Eble, H. O. Mofjeld, J. C. Newman, and A. J. Venturato. Real-Time Tsunami Forecasting: Challenges and Solutions. *Natural Hazards*, 35:41–58, 2005. [1](#), [22](#)
- [THT02] M. I. Todorovska, A. Hayir, and M. D. Trifunac. A note on tsunami amplitudes above submarine slides and slumps. *Soil Dynamics and Earthquake Engineering*, 22:129–141, 2002. [7](#)
- [TS98] V. V. Titov and C. E. Synolakis. Numerical modeling of tidal wave runup. *J. Waterway, Port, Coastal, and Ocean Engineering*, 124:157–171, 1998. [14](#)
- [TT01] M. I. Todorovska and M. D. Trifunac. Generation of tsunamis by a slowly spreading uplift of the seafloor. *Soil Dynamics and Earthquake Engineering*, 21:151–167, 2001. [1](#), [7](#), [9](#)
- [Vol07] V. Volterra. Sur l’équilibre des corps élastiques multiplement connexes. *Annales Scientifiques de l’Ecole Normale Supérieure*, 24(3):401–517, 1907. [4](#)
- [Whi99] G. B. Whitham. *Linear and nonlinear waves*. John Wiley & Sons Inc., New York, 1999. [10](#), [14](#)
- [WL08] S. A. Weinstein and P. R. Lundgren. Finite Fault Modeling in a Tsunami Warning Center Context. *Pure Appl. Geophys.*, 165:451–474, 2008. [2](#), [22](#)
- [XG09] L. Xu and P. Guyenne. Numerical simulation of three-dimensional nonlinear water waves. *J. Comput. Phys.*, 228(22):8446–8466, 2009. [13](#)

- [Yal08] A. C. Yalciner. July 17, 2006 Indonesia Java Tsunami. Technical report, <http://yalciner.ce.metu.edu.tr/java/>, 2008. 3
- [Zak68] V. E. Zakharov. Stability of periodic waves of finite amplitude on the surface of a deep fluid. *J. Appl. Mech. Tech. Phys.*, 9:1990–1994, 1968. 10, 25

LAMA, UMR 5127 CNRS, UNIVERSITÉ DE SAVOIE, CAMPUS SCIENTIFIQUE, 73376 LE BOURGET-DU-LAC CEDEX, FRANCE

E-mail address: `Denys.Dutykh@univ-savoie.fr`

URL: <http://www.lama.univ-savoie.fr/~dutykh/>

IMA, UNIVERSITY OF MINNESOTA, MINNEAPOLIS, MN 55455, USA

URL: <http://sites.google.com/site/dmitsot/>

LAMA, UMR 5127 CNRS, UNIVERSITÉ DE SAVOIE, CAMPUS SCIENTIFIQUE, 73376 LE BOURGET-DU-LAC CEDEX, FRANCE

E-mail address: `Xavier.Gardeil@etu.univ-savoie.fr`

SCHOOL OF MATHEMATICAL SCIENCES, UNIVERSITY COLLEGE DUBLIN, BELFIELD, DUBLIN 4, IRELAND

E-mail address: `frederic.dias@ucd.ie`